

**MAPPING LATERAL EXTENT OF SUEVITES AT NORTHERN
PART OF LAKE BOSUMTWI USING RESISTIVITY AND
SEISMIC REFRACTION METHODS**

BY
KNUST

Emmanuel HABIMANA

(BSc. Applied Physics)

**A thesis submitted to the Department of Physics, Kwame Nkrumah
University of Science and Technology in partial fulfillment of the
requirements for the degree of**

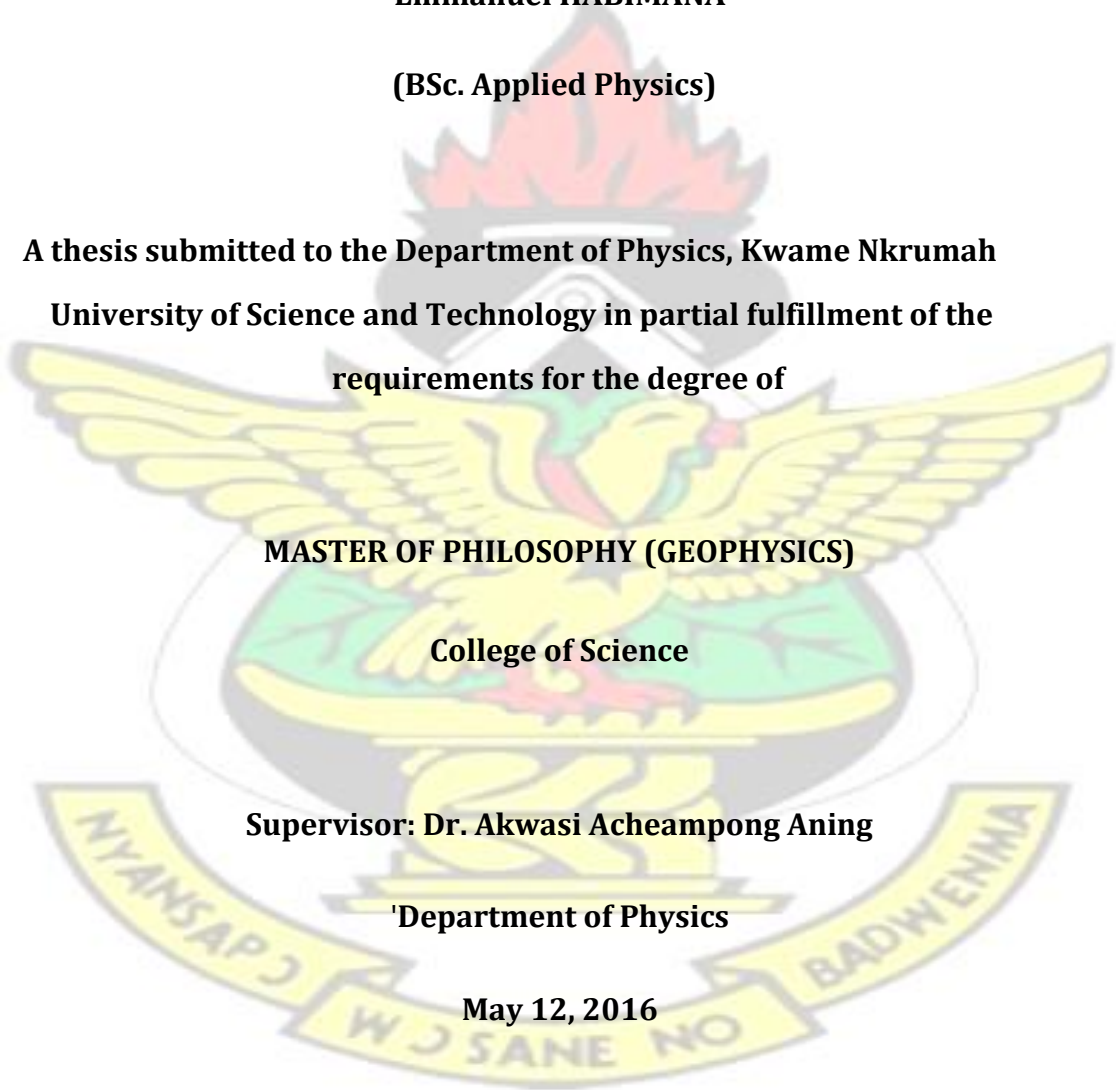
MASTER OF PHILOSOPHY (GEOPHYSICS)

College of Science

Supervisor: Dr. Akwasi Acheampong Aning

Department of Physics

May 12, 2016



Declaration

I hereby declare that this submission is my own work towards the award of MPhil degree and that, to the best of my knowledge, it contains no material previously published by another person or material which has been accepted for the award of any degree of the university, except where due acknowledgement has been made in the text.

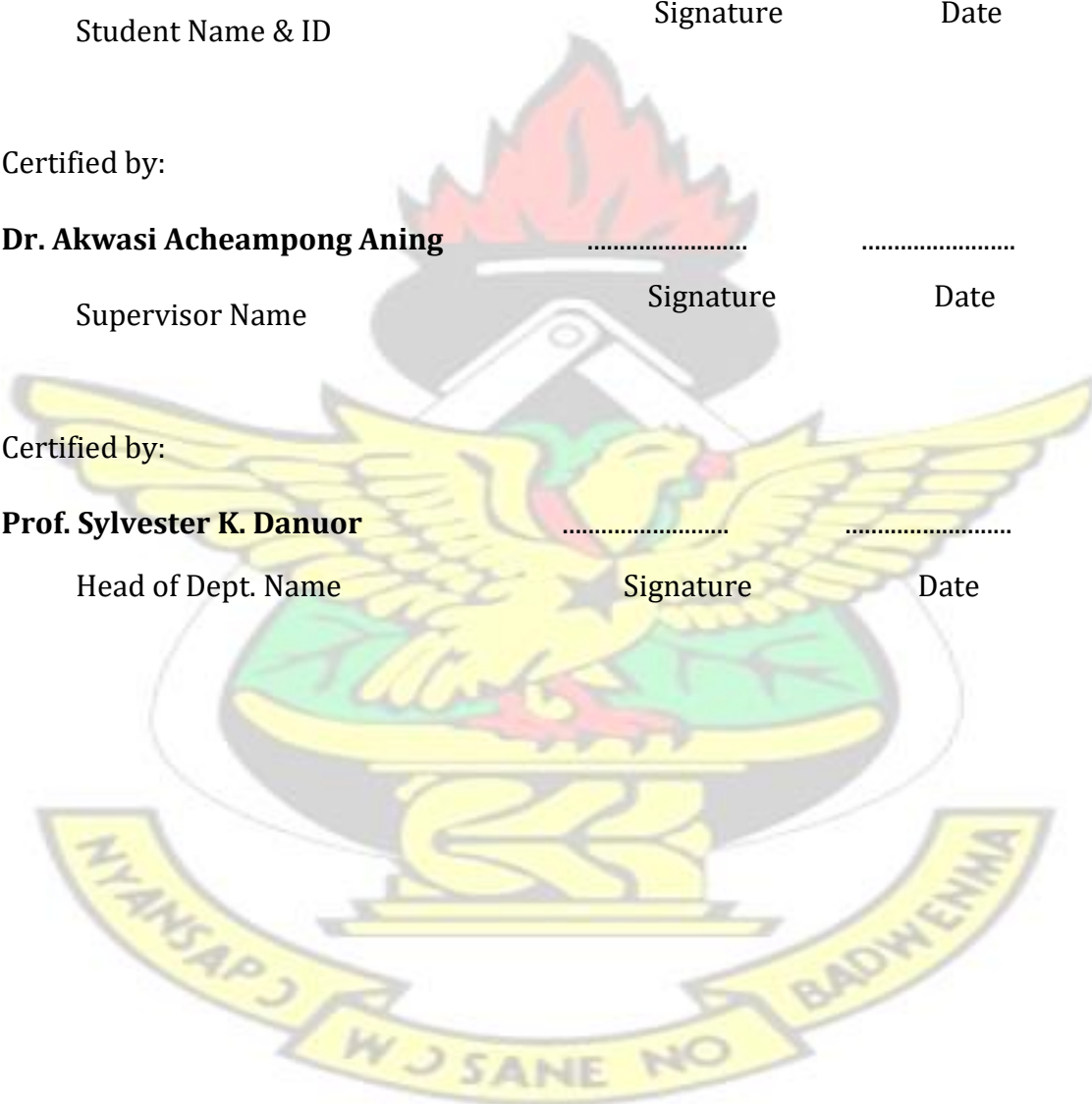
Emmanuel HABIMANA (20436656)
Student Name & ID Signature Date

Certified by:

Dr. Akwasi Acheampong Aning
Supervisor Name Signature Date

Certified by:

Prof. Sylvester K. Danuor
Head of Dept. Name Signature Date



KNUST

Abstract

Electrical resistivity imaging and seismic refraction method have been used to map the lateral extent of suevites in northern lake of Bosumtwi. Seven electrical resistivity tomography and two seismic refraction profiles were surveyed. The lengths of the profiles varied between 160 and 600 m. The multi electrode system was combined with roll along techniques for resistivity data collection using gradient array. Roll along was also executed for the seismic refraction survey where two geophones were overlapped to extend the survey length. The data was acquired in 2D where 4 m as electrodes separation was also equal to geophones spacing, while shooting interval was 8 m. Depth of investigation for resistivity and seismic refraction surveys are 25 m and 26 m respectively. Data was processed

with Res2dinv and ReflexW for the resistivity and seismic refraction respectively. Electrical resistivity and seismic refraction tomography identified fractured zones as well as suevite deposits which were observed within 12 m depth. Resistivity of northern Bosumtwi suevites varies between 1.56 and 25 Ωm , and the P wave velocity ranges from 3000 to 3900 m/s. The results also showed that the subsurface is made up of either two or three layers: unconsolidated top soil and moist clay, soil with moisture content or clayey soil and fractured claystone. The seismic refraction tomography and the electrical resistivity tomography agree well in revealing subsurface geological units based on their velocity and resistivity values.



KNUST



Contents

Declaration	i
Abstract	ii
List of Tables	vi
List of Figures	vi
List of Symbols and Acronyms	x
Acknowledgements	xii
1 INTRODUCTION	1
1.1 Introduction	1
1.2 Literature review	5
1.2.1 Formation of craters	5

1.2.2	Impact derived rocks (Impactites)	7
1.2.3	Previous studies	8
1.3	Problem statement	10
1.4	Project objectives	10
1.4.1	General objective	10
1.4.2	Specific objectives	10
1.5	Justification of research	11
1.6	Scope of the project	11
1.7	Thesis layout	12
2	GEOLOGY	13
2.1	Regional geology	13
2.1.1	Introduction	13
2.1.2	Proterozoic birimian supergroup	14
2.1.3	The Tarkwaian System	18
2.1.4	Volta Basin sediments	19
2.2	Local geology	19
2.2.1	Geology of the survey site	19
3	THEORETICAL BACKGROUND	24
3.1	The seismic refraction method	24
3.1.1	Introduction	24
3.1.2	Main assumption and limitations of the seismic refraction method	25
3.1.3	Seismic waves	25
3.1.4	Body waves	27
3.1.5	Ray path of seismic refracted wave	28
3.1.6	Dipping layer	33
3.1.7	Discontinuity layer	36

3.2	The resistivity method	37
3.2.1	Introduction	37
3.2.2	Basic dc resistivity principles	37
3.2.3	The geology and resistivity	41
3.2.4	Electrode configuration	42
3.2.5	Depth of current penetration	45
3.2.6	Modes of electrical resistivity surveying	45
4	METHODOLOGY	49
4.1	Introduction	49
4.2	Data acquisition	49
4.2.1	Seismic refraction survey	49
4.2.2	Electrical resistivity survey	54
4.3	Data processing	58
4.3.1	Seismic refraction field data	58
4.3.2	Electrical resistivity field data	59
5	RESULTS AND DISCUSSIONS	62
5.1	Introduction	62
5.2	2D resistivity models	63
5.3	Seismic refraction models	72
6	CONCLUSION AND RECOMMENDATIONS	78
6.1	Conclusion	78
6.2	Recommendations	80
	Appendix	89

List of Tables

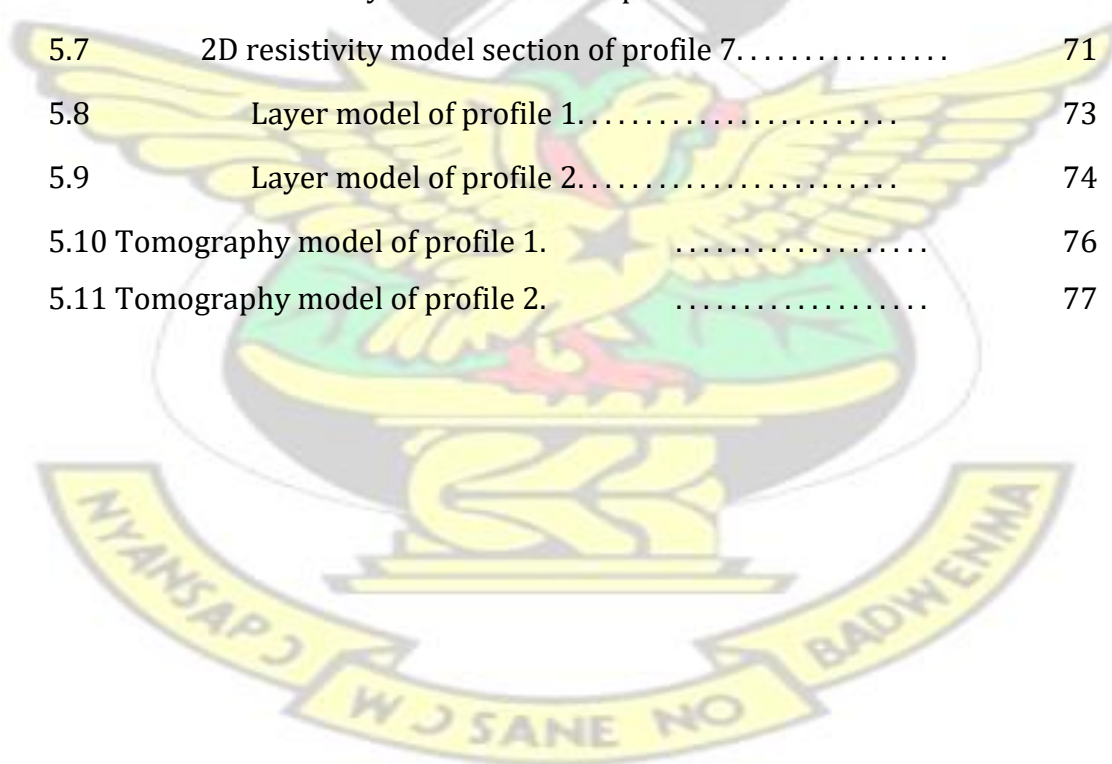
2.1	Division of the metasedimentary Birimian, (adapted from (Asihene and Barning, 1975)).	16
2.2	Divisions of the Meta-volcanic Birimian (adapted from (Asihene and Barning, 1975)).	16
2.3	Division of Tarkwaian (adapted from (Junner, 1940)).	18
3.1	Examples of P-waves velocities (Reynolds, 2011).	30
3.2	Resistivity values of common geologic materials from Telford et al. (1990) and Reynolds (2011).	44
4.1	List of acquisition parameters.	51

List of Figures

1.1	Panoramic view of the Bosumtwi impact crater (Koeberl et al., 2007).	2
1.2	Bosumtwi crater location relative to the Ivory Coast tektite strewn field from (Koeberl et al., 1998).	3
1.3	Location of Bosumtwi suevites relative to crater.	4
1.4	Suevitic outcrops in the study area.	4
1.5	Cross section of a simple crater (French et al., 1997).	6
1.6	Cross section of a complex crater (French et al., 1997).	7
2.1	Location of study area relative to geological map of Ghana (adapted from Duodu (2009)).	15
2.2	Simplified geological map of the Bosumtwi impact structure (Jones et al., 1981; Koeberl et al., 1998; Reimold et al., 1998).	20
2.3	Stratigraphic column for 2 drill holes through suevites (Boamah	

and Koeberl, 2003).....	23
3.1 Reflection and refraction of (a) obliquely incident ray and (b)normal incident ray adapted from Telford et al. (1990)	28
3.2 Simplified cartoon example of seismic refraction. Propagation of the waves according to Huygens's principle.	31
3.3 Travel time distance curves for 3 horizontal layers; modified from Reynolds (2011).	32
3.4 (a)Raypath geometry over a refractor dipping at angle(α) and (b)travel time-distance graph for forward and reverse shooting di- rections,(Reynolds, 2011)	34
3.5 (a) Raypath geometry over a boundary with a step discontinuity but no lateral change in velocity and (b)the travel time-distance graph (Reynolds, 2011).	36
3.6 Variations in electric current density due to the variation in sub- surface resistivity (Griffiths and Barker, 1993).....	38
3.7 Current injection into a wholespace of uniform resistivity from Ev- erett (2013).....	39
3.8 Generalized form of electrode configuration in resistivity surveys modified from, Knoedel et al. (2007).....	40
3.9 Electrode configurations and their apparent resistivity formulas, adapted from Loke (1999) and Reynolds (2011).....	43
3.10 2D resistivity surveys with 3 electrode quadripole combinations using Wenner array adopted from (Loke and Lane Jr, 2004)....	47
3.11 The use of the roll-along technique to extend the area covered by a 2-D resistivity survey (Loke and Lane Jr, 2004).....	48
4.1 Survey design.	50
4.2 (a)The set up of Terraloc MK6 System, (b) Data acquisition with the terraloc MK6 system along a profile.	52

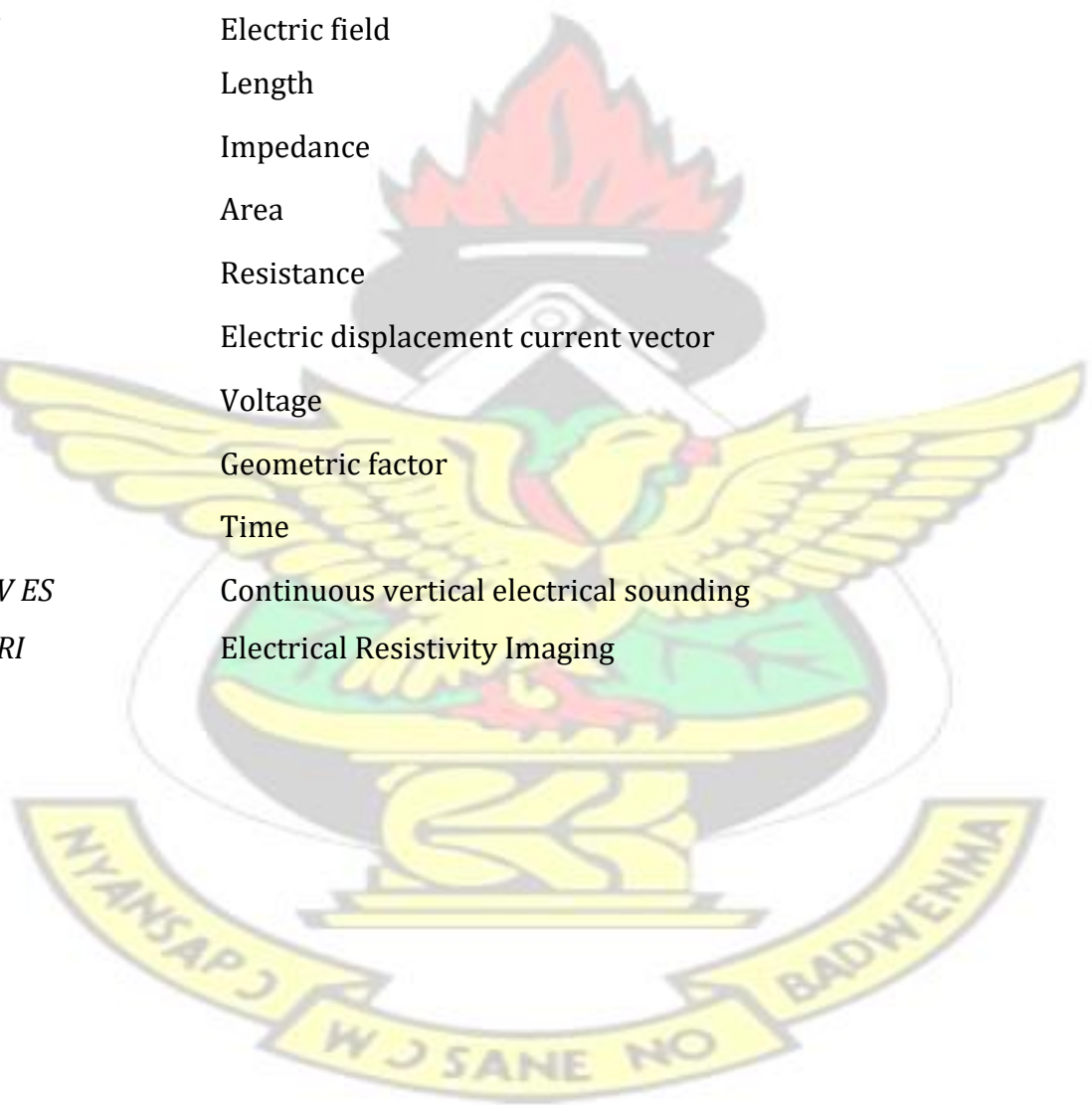
4.3	Roll along technique during seismic refraction survey.....	53
4.4	(a and b) Data acquisition with the ABEM LUND imaging system along a profile, (c) elevation measurement with GPS.....	55
4.5	Sketch of odd numbered take-outs connection with electrodes. . .	56
4.6	Data acquisition process using roll-along technique.....	57
4.7	First arrival travel time picking.....	58
4.8	Pseudosection with bad data points (marked with red crosses)...	61
5.1	2D resistivity model section of profile 1.....	64
5.2	2D resistivity model section of profile 2.....	66
5.3	2D resistivity model section of profile 3.....	67
5.4	2D resistivity model section of profile 4.....	69
5.5	2D resistivity model section of profile 5.....	69
5.6	2D resistivity model section of profile 6.....	71
5.7	2D resistivity model section of profile 7.....	71
5.8	Layer model of profile 1.....	73
5.9	Layer model of profile 2.....	74
5.10	Tomography model of profile 1.	76
5.11	Tomography model of profile 2.	77



List of symbols and acronyms

<i>ERT</i>	Electical Resistivity Tomography
<i>SRT</i>	Seismic Refraction Tomography
π	3.14
<i>SI</i>	System international units
<i>D</i>	Diameter of crater
<i>c</i>	Speed of light in vacuum
V_p	Primary wave velocity
V_s	Shear wave velocity
<i>E</i>	Young's modulus
<i>K</i>	Bulk modulus
μ	Shear modulus
$\tan(\theta)$	Shear strain
<i>P</i>	Pressure
<i>X</i>	Horizontal distance
<i>Z</i>	Depth
ρ	Density
A_0	Amplitude of incident wave
A_1	Amplitude of reflected wave
A_2	Amplitude of refracted wave
<i>T</i>	Transmission coefficient
<i>R</i>	Reflection coefficient
θ_c	Critical angle
α	Angle of dip
V_u	Apparent velocity for up dip direction
V_d	Apparent velocity for down dip direction
Ω	Ohms

σ	Poisson's ratio
ρ	Resistivity
ρ_a	Apparent Resistivity
φ	Porosity
S	Saturation
I	Electric current
\vec{J}	Electric current density
\vec{E}	Electric field
L	Length
Z	Impedance
A	Area
R	Resistance
\mathbf{D}	Electric displacement current vector
V	Voltage
K	Geometric factor
t	Time
$CVES$	Continuous vertical electrical sounding
ERI	Electrical Resistivity Imaging



KNUST

Acknowledgements

My first and foremost acknowledgement goes to the Almighty Jehovah God for His protection and abundant love throughout this programme. I wish to acknowledge KNUST for admitting me to pursue the MPhil geophysics programme. Special and heartfelt thanks to my supervisor, Dr. Akwasi Acheampong Aning for his continuous encouragement, constructive criticisms and kind assistance throughout this project from data acquisition to the software I used in data processing.

Many thanks to Mr. Vandycke Asare Sarpong for his support and guidance during the data collection. I am grateful to Mr. Callistus Nero and Mr. Thomah Dwomah (the geophysics technician) who usually left their work and went to the field with us throughout the data acquisition period. I don't think that I can repay them for their generosity, but God bless their endeavours. Also many thanks to Dr. Ernest Ohene Asare and Dr. David Wemmegah for introducing me to Linux and MapInfo respectively. Thanks to the Bosumtwi local community who allowed me to carry out the geophysical survey on their land.

Great appreciation is also rendered to all physics department lecturers (KNUST) for their warm cooperation and kind assistance throughout this programme. Sincere thanks to all classmates for their kind collaboration throughout this

programme. I am deeply indebted to the international programmes office of KNUST for their continuous encouragement especially Prof William Oduro and Madam Vanessa Appiah. My sincerest thanks to the commonwealth secretariat for offering me a scholarship to pursue the geophysics programme, as well as the university of Rwanda college of science and technology for giving me a study leave.

KNUST



Chapter 1

INTRODUCTION

1.1 Introduction

The Bosumtwi impact crater is a huge research site in Ghana as well as in the World. It is one youngest complex impact crater that was formed by a meteorite impact about 1.07 ± 0.05 Ma. The lithology of target area is mostly formed by Proterozoic (2.1-2.2 Ma years) of Birimian supergroup that consists of lower greenschist facies metasediments, graywackes, schists, quartzites, phyllites, and a minor granitic component (Wright, 1986; Koeberl et al., 1997; Leube et al., 1990). It is situated at $06^{\circ}32'0''$ N, $01^{\circ}25'0''$ W about 32 km Southeast of Kumasi in the Ashanti Region of Ghana (Koeberl et al., 1998, 2007). The crater which is occupied by lake Bosumtwi (Figure 1.1), has an average diameter of about 10.5 km (Junner, 1940; Jones, 1985). The Lake Busumtwi itself however, which is closed in terms of hydrology, has a diameter and depth of about 8.5 km and 75 m respectively (Scholz et al., 2002).

Around the world, there are 188 confirmed impact structures (Spray and Hines, 2009). Thus, Bosumtwi crater is one of nineteen confirmed African impact craters as well as one of impact craters associated with tektite strewn field (Koeberl et al.,

1997; Spray and Hines, 2009). It is surrounded by a rim with diameter about 20 km with an elevation ranging from about 250 to 300 m from the lake surface (Jones et al., 1981; Reimold et al., 1998; Garvin et al., 1992; Wagner et al., 2002).

There are similarities in isotropic and chemical compositions, as well as the range of age for Bosumtwi impact glasses and Ivory Coast tektites. Bosumtwi impact crater is taken as the source of Ivory Coast tektites (Figure 1.2) (Lacroix, 1934; Glass, 1969; Gentner et al., 1969; Koeberl et al., 1998). Tektites are natural glasses

occurring on Earth which have been developed by hypervelocity impact melting from terrestrial upper-crustal rocks. Tektites exist in four different strewn fields namely; Australasian, Ivory Coast, Central European as well as North American (Koeberl, 1986, 1994). Tektites are usually located away from the source of the crater; they are therefore referred as distal ejecta.

Impactites are formed during the meteorite impact process, from the shocked impact rocks, such as monomict/polymict breccias. The suevites are polymictic clastic matrix breccia containing glass fragments, rocks, mineral and clasts component of impact melt exhibiting various stages of shock metamorphism (Stöffler and Grieve, 1994). Suevites are one of the polymict breccias forming the impactite lithologies at Bosumtwi crater. During the meteorite impact they have been thrown to the North and South-West of impact center which is currently filled with lake Bosumtwi (Figure 1.3) (Junner, 1940; Jones et al., 1981). The northern part of Bosumtwi suevites were the interest of this study and figure(1.4) shows suevitic outcrops. It occupies an area of about 1.5 km^2 ; moreover, the drill core result revealed that their thickness is less or equal to 15 m (Boamah and Koeberl, 2003). Strictly speaking, the studies on impact craters contribute useful information about planetary and terrestrial environment, including biosphere.



Figure 1.1: Panoramic view of the Bosumtwi impact crater (Koeberl et al., 2007).

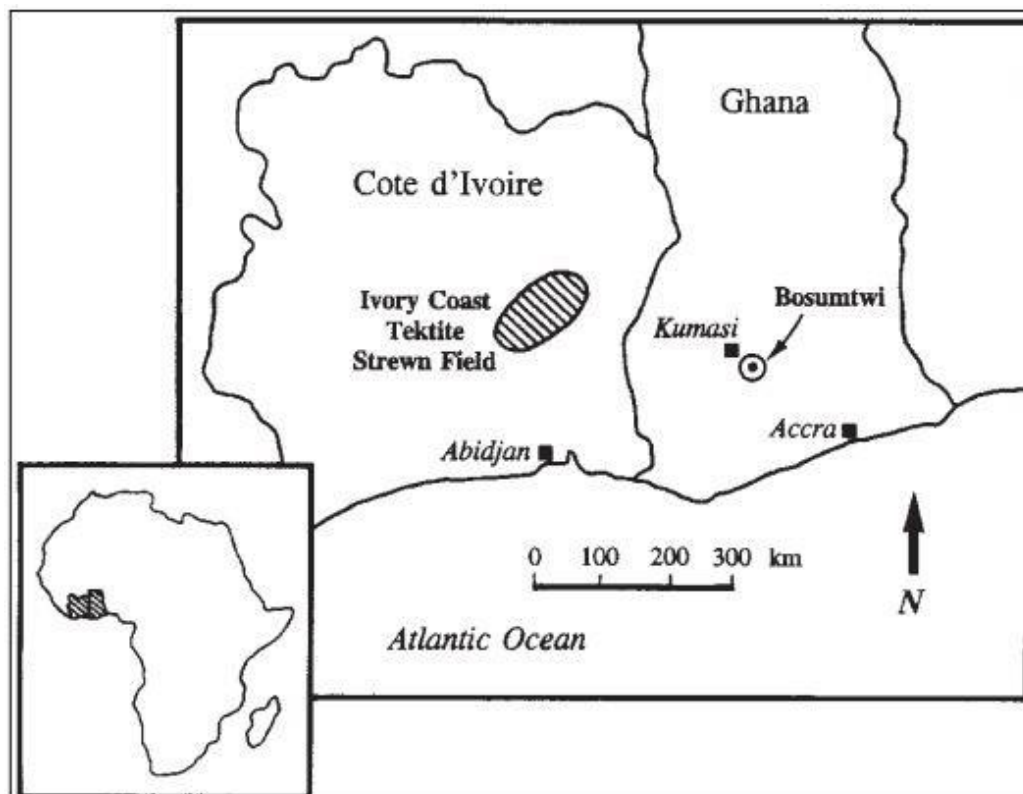


Figure 1.2: Bosumtwi crater location relative to the Ivory Coast tektite strewn field from (Koeberl et al., 1998).

Therefore, non-invasive geophysical methods were used in this project to map the northern Bosumtwi suevite deposits. The presence of cocoa farms, tropical forest and bushes as well, made the survey more complicated. Since the 20th century, geophysical methods have become the most applied techniques in environmental and engineering investigations. It has been mostly depending on their main characteristics, such as flexibility, non-invasiveness, low cost and fast acquisition of high resolution data and the possibility to investigate a large area (Jongmans and Garambois, 2007).

Geophysical survey techniques can be used in mining, impact cratering, hydrology and environmental studies. They are broadly defined as non-invasive and nondestructive methods used for imaging and mapping subsurface features based on physical property contrast. They have been used as techniques for subsurface study for better understanding of the geophysical responses due to the physical property contrast.

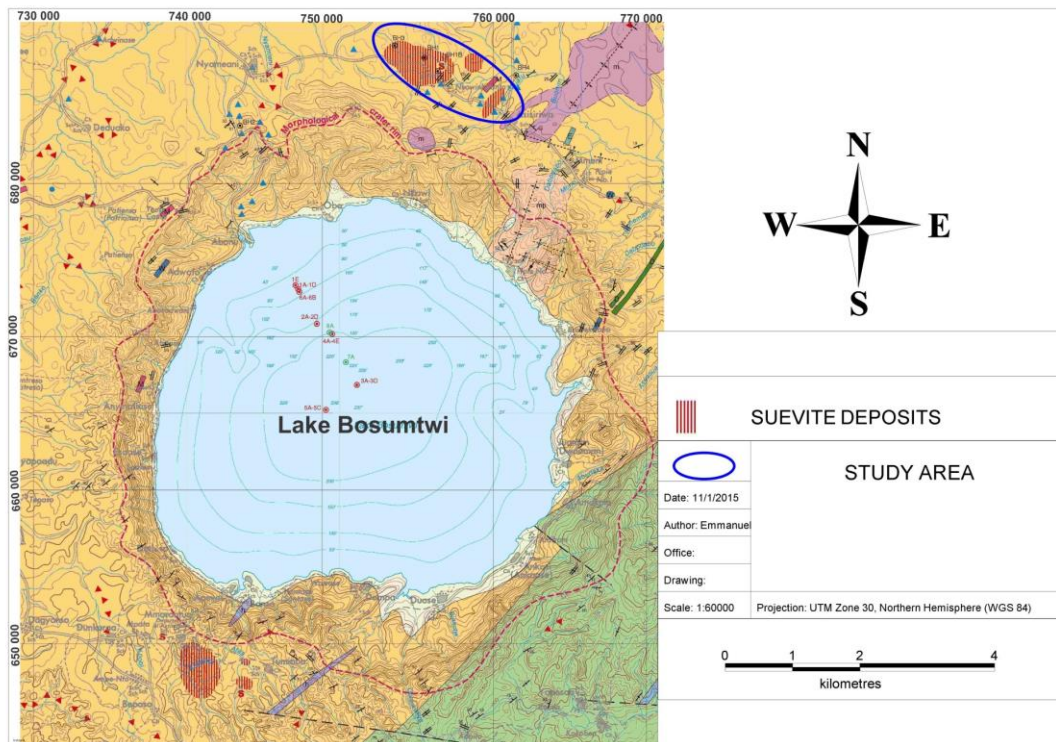


Figure 1.3: Location of Bosomtwi suevites relative to crater.



Figure 1.4: Suevitic outcrops in the study area.

Since suevites are considered generally as brecciated mixture of melted materials, they have density and electrical resistivity contrast with the surrounding region. In addition to the compaction of the material; porosity, fractures, fluid content of the material are the petrophysical parameters controlling measurable quantities such as seismic velocity, electrical resistivity, among others.

For optimum results an integration of geophysical methods is often advised, and this study combines electrical resistivity tomography (ERT) and seismic

refraction tomography(SRT) to reveal underlying structures such as faults, fractures and suevite deposits in the northern part of lake Bosumtwi.

Seismic investigations can be conducted for geological and engineering purposes.

Seismic refraction method depends on the transmission of seismic wave through a medium. Two-dimensional electrical surveys should be used in conjunction with seismic methods or GPR surveys as they provide complementary information about the subsurface (Loke and Lane Jr, 2004). For instance, seismic refraction method can map undulating interfaces well, but will have difficulty in mapping discrete bodies such as boulders, cavities and pollution of plumes. GPR surveys can provide more detail pictures but have very limited depth penetration in the areas with conductive unconsolidated sediments (clays soils).

ERT is the most efficient technique of the electrical resistivity method used to map the subsurface areas of complex geology. In ERT method, the sounding and the profiling techniques are integrated to give information on both the lateral and the vertical extents of the subsurface. During electrical resistivity survey, four metals called electrodes are planted into the ground. Electrical current is introduced using two electrodes, and the electrical potential between two other electrodes is simultaneously measured.

1.2 Literature review

1.2.1 Formation of craters

The Bosumtwi structure has been confirmed as an impact crater since 1931 (Maclaren, 1931). It was later confirmed by many evidences, especially, the presence of shock metamorphism, impact melt as well as coesite in suevites (Littler et al., 1961; Jones et al., 1981; Koeberl, 1994).

Impact craters are a result of a collision of two cosmic bodies of very different sizes; and it can be referred to as impact on the surface if the target is Earth. Impact cratering is one of the most important geological processes that modify the morphology of terrestrial planet's surface and subsurface.

Impact structures and impact derived rocks (impactites) are formed as a result of high temperature and pressure of the hypervelocity of meteorite. Some impactites however, are thrown away from the source (distal ejecta) and deposited in different locations around the crater. In addition, the shock waves generated by impacts can cause the formation of new subsurface structural features around the target. These phenomena cause the changes in stratigraphy or lithology of the subsurface that may induce the physical property contrasts which the geophysical methods are sensitive (Melosh, 1989; French et al., 1997). Impact craters can be subdivided into two main distinct types, simple and complex craters. Simple craters are small craters of diameter less or equal to 4 km. They are also characterized by a bowl-shaped features in which the final structures are almost the same as the transient crater shape as shown in figure 1.5, where D, d_a, d_t stand for diameter, apparent diameter of the crater and true diameter respectively.

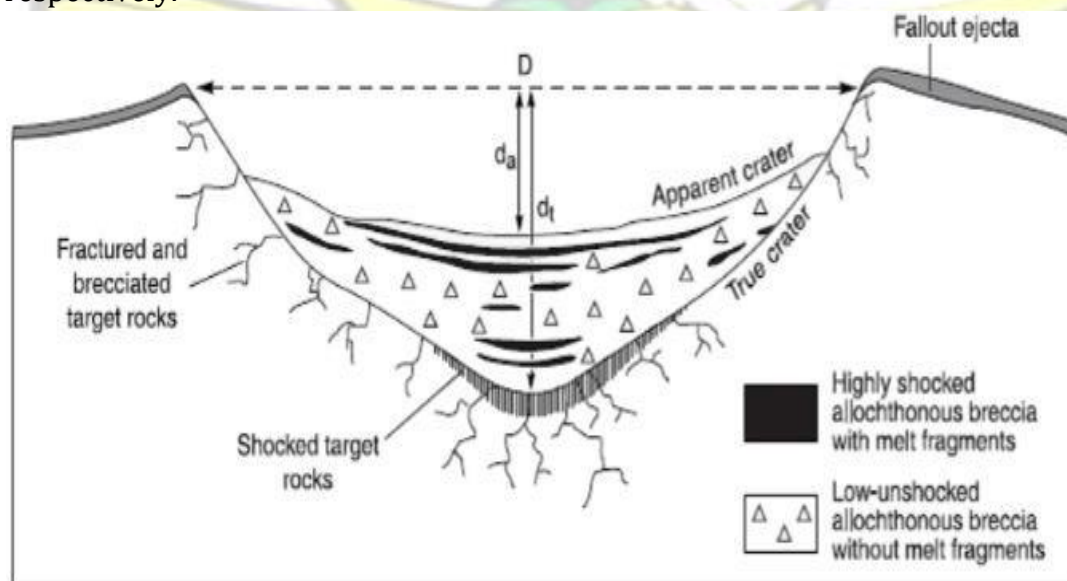


Figure 1.5: Cross section of a simple crater (French et al., 1997).

Complex craters are characterized by a central uplift induced by the elastic rebound of the crater floor in modification stage and by the circular depression around it (Figure 1.6), where D is the diameter of the crater from rim to rim. Furthermore, for the complex crater, the central uplift shows a basin in its center.

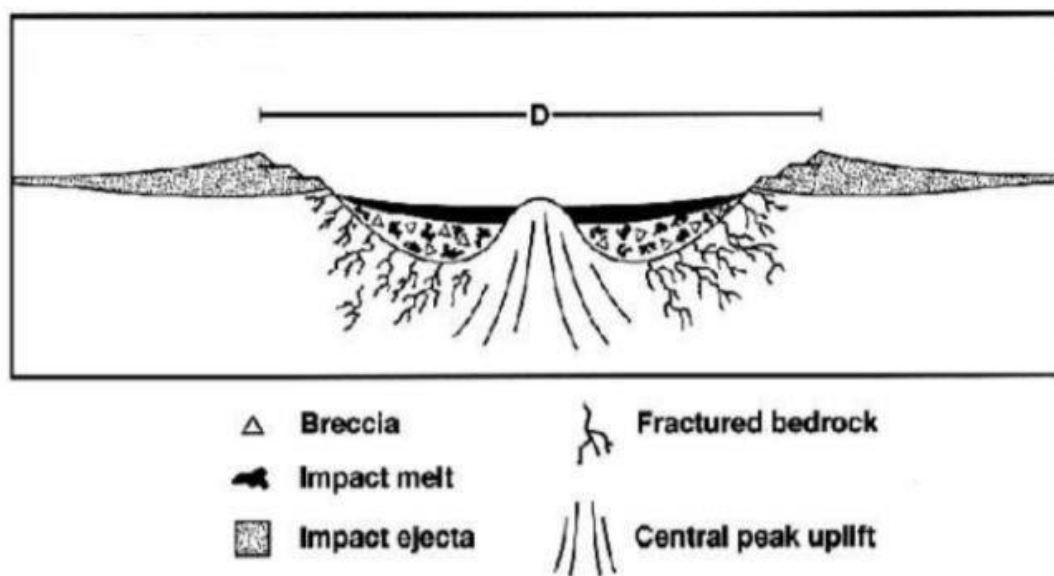


Figure 1.6: Cross section of a complex crater (French et al., 1997).

1.2.2 Impact derived rocks (Impactites)

The high temperature and pressure produced by hypervelocity of meteorite lead to the formation of new rocks. These rocks formed from terrestrial target rocks are generally known as impactites (impact derived-rock). Impact breccias are one of the examples of impactites. They are therefore breccias containing lithic and mineral clast excavated from the target rocks. They deposit in or around the crater, sometimes they can also be injected as dykes into the original target rocks (Koeberl et al., 1998, 1997).

The impact breccias are subdivided into two main types namely monomict and polymict breccias. If all clasts come from the same source of rock type, the impact breccias are known as monomict breccias (autochthonous breccias). However, if the clasts are made up of several rock types, the impact breccias are called polymict (allochthonous) breccias. Therefore, the polymict breccias that exhibit some impact melts or glass particles are known as suevites. They were first found at Ries crater in Southern Germany (Stöffler and Grieve, 1994).

In addition to the suevites, other important materials generated by impacts are tektites and microtektites. They are simply defined as small particles of glass formed through the melting of target rocks and thrown out by force of the impact,

often over thousands of kilometer squared (Koeberl et al., 1998; Reimold et al., 1998).

1.2.3 Previous studies

Studies by French et al. (1997) on Barringer (Meteor) crater in Arizona have revealed that the impact process has an important geological phenomenon. Fragments of Coconino sandstone ejected off the crater show a whole range of shock from normal detritic texture, strong fracturing and crushing, intense deformation of quartz grains, resulting in cleavage, and complete fusion of sandstone producing the vesicular pumice-like rock containing 95% silica including hyperbolic silica polymorph coesite and stishovite (Chao, 1968).

In addition to coesite and stishovite Chao (1968), Ries crater in Germany contains planar features like quartz and feldspar as well as pure silica glass. Studies by Garvin et al. (1992) based on new outcrops of suevite in the Ries crater have revealed that the suevite layer is divided into main suevite rich in pancake shaped bombs and relatively well sorted thin base suevite consisting of fine gravel and bubble containing angular glass segments.

The physical properties induced in impactites (impact derived-rocks) are different from its vicinity unshocked bedrocks. Studies carried out in Bosumtwi meteorite impact structure, by Plado et al. (2000), revealed the difference in physical properties of pre-impact early proterozoic metasediments (target rocks) and melt-rich suevite (impactites). They found out that the suevites have low density about 2040 kg/m^3 , high porosity about 25% and high magnetization (magnetic susceptibility about $330 \times 10^{-6} \text{ SI}$) relative to the target rock: density about 2510 kg/m^3 ; porosity about 8% as well as magnetic susceptibility about $150 \times 10^{-6} \text{ SI}$. Boamah and Koeberl (2003) found that the thickness of the suevites deposit is less or equal to 15 m.

Electrical resistivity method was used during the geophysical studies in *Kardla* impact structures in Estonia (Plado et al., 1996). Their work revealed that the difference in resistivity is generally caused by an impact induced increase of

porosity and fluid content in impactites. Plado et al. (1996) found that water saturated drill core samples show low resistivity values for impact breccias about $5500 \Omega m$ and fractured basement granites about $2500 \Omega m$ as compared to target granites about $100 k\Omega m$. They also realized that the resistivities of fractured granites from the upper part of the central uplift and rim wall were $21 k\Omega m$ and $15 k\Omega m$ respectively. Therefore, the higher resistivity in the central part was attributed to less fractured uplifted granitic rocks.

Seismic refraction methods have been used as well in subsurface impact structures investigations (Pilkington and Grieve, 1992). They have been used to characterize the horizontal and vertical extent of shock induced fracturing in autochthonous breccias (Ackermann et al., 1975) and to approximate the thickness of the allochthonous breccia lens and to characterize the central uplift (Green and Chetty, 1990).

The seismic methods were first used on the lake Bosumtwi impact crater by Karp et al. (2002). The stratigraphy of Bosumtwi impact crater in terms of 2D velocity model, was divided into 4 layers. First layer of water with average velocity of 1.45 km/s ; followed by postimpact sediments layer with seismic velocity varying from 1.5 to 1.9 km/s . The third layer is made of allochthonous breccia and suevites (brecciated rocks layer) with seismic velocity ranging from 2.5 to 3.5 km/s . The fourth one is the crater floor layer, formed by fractured target rock, with average seismic velocity of 3.8 km/s (Karp et al., 2002; Danuor et al., 2013).

ERT studies by Aning et al. (2013b) in the inner wall of the crater revealed the direction of the meteorite. The average of the angle of dip of faults and fractures delineated by Aning et al. (2013b) are about 60° in east and 80° west section of crater; which were also consistent with the results of Reimold et al. (1998), and Hunze and Wonik (2007). They also found that the direction of dip of sediment/bedrock contact varies from 16° in the northeast to 36° in the southwest. Since there was an increase in the angle of dip towards the southwest, Aning et al.

(2013b) found that the meteorite was an oblique impactor from northeast.

1.3 Problem statement

The energy of hypervelocity of meteorite usually causes different effects on the surface target, like deformation of the subsurface and formation of new rocks. These rocks are generally known as impactites. The impactites at the Bosumtwi crater consist of suevitic breccias. However, the lateral extent of suevites is still a subject of discussion. Although the geologists have mapped out the suevites, the continuous in-situ geophysical studies are still needed in order to confirm or improve the geological findings. The previous studies about suevites deposit were a point and random based.

1.4 Project objectives

1.4.1 General objective

The main objective of this research is to map the subsurface distribution of suevite deposits in northern part of Lake Bosumtwi using a combined electrical resistivity tomography and seismic refraction tomography methods.

1.4.2 Specific objectives

- (i) To map the thickness of the northern Bosumtwi suevites,
- (ii) To map subsurface strata and fractured zones,
- (iii) To determine the resistivity and p-wave velocity of the suevites

1.5 Justification of research

Bosumtwi impact crater has become a national and international research site, due to its complex subsurface modifications. The first geophysical study that was carried out in suevite deposits was by drilling a boreholes (Boamah and Koeberl, 2003; Koeberl et al., 2007). In addition to time consuming and high cost of drilling, it provided only insight of a restricted space. Hence, in this research a combination of ERT and SRT methods which were less expensive and less time

consuming were used to map suevite deposits, and their vicinity subsurface deformations.

These geophysical methods are suitable for subsurface characterization because, they generate a continuous image of the subsurface in two dimensions, significantly reducing the risk of undetected geologic formation. Geophysical mapping of suevites, will provide useful information about the Earth's environment and impact cratering science.

The suevites usually contain a high percentage of the elements that are normally present in meteorites as compared to the surrounding terrestrial rocks. The presence of suevites at impact crater sites is one of the criteria for an origin of the crater by meteorite impact. Their location and distribution at impact at impact crater sites are important since they can be used as constraints in modeling the direction the impact direction of the planetary body.

1.6 Scope of the project

This research is limited to mapping the suevite deposits of the northern part of Lake Bosumtwi and subsurface geological units in their vicinity. Currently, this deposit is divided into two parts by ASISIRIWA – NYAMIANI main road.

1.7 Thesis layout

This thesis has six chapters and each of them addresses a major heading of the thesis. Chapter 1 introduces historically and geologically the site of this research. It explains briefly geophysical methods that have been applied during data acquisition. Chapter 1 also deals with objectives and justification of this research; related previous studies were also reviewed in this chapter.

Chapter 2 explains general overview of the regional and local geological information of the research site. Theoretical background and working principles of electrical resistivity tomography as well as seismic refraction methods are outlined in chapter 3.

Chapter 4 explains how these geophysical methods were implemented during data acquisition. Processing steps also are detailed in this chapter. The results are discussed and presented in various models in chapter 5; while chapter 6 deals with conclusion of findings and makes recommendations to the future researchers.

KNUST



Chapter 2

GEOLOGY

2.1 Regional geology

2.1.1 Introduction

Ghana lies largely within the West African Shield or Craton. The West African Shield is subdivided into three age provinces. The **oldest part** is formed by Archean rocks in Sierra Leone, Liberia, as well as Guinea and is called the *Liberian Craton*. The **central part** consists of Ivory Coast, Ghana, and Burkina Faso and is mostly formed by the Birimian supracrustals. The **Eastern part**, where you find Benin, Togo, Nigeria, Chad, as well as Niger; the shield is dominated by Archean-age basement complexes and Proterozoic supracrustals (Kesse, 1985; Leube et al., 1990).

Figure 2.1 shows the geology of Ghana. The subsurface is composed of metamorphosed rocks of Paleoproterozoic age that fall mainly within the age range of 2300 to 1900 Ma. Geologically, on the basis of lithologic, tectonic and age of supracrustal rocks, Ghana can be divided into five geological provinces (Hastings, 1982). These are:

The western unit which lies at the eastern margin of the Precambrian West African Shield.

The southeastern unit which is at the southeastern part of the country belonging to the Precambrian Mobile Belt.

The flat lying unit which is made up mainly of the sediments of the Voltaian basin.

The coastal basins and,

Tertiary to recent deposits.

2.1.2 Proterozoic birimian supergroup

The very thick and extensive sequence of supracrustals metamorphosed sediments and volcanic rocks in Ghana are called Birimian, after the Birim region in Southern Ghana where the rocks were first found. The Birimian Supergroup System in Ghana, consists of **meta-sediments** and **meta-volcanics**. The results from radiometric age dating of detrital grains of Birimian units, fall in the range within 2180 to 2130 Ma (Davis et al., 1994; Yao et al., 2001). The metamorphic grades vary from greenschist to almandine-amphibolite facies which are mainly a source of diamonds and manganese ores.

The metasediment Birimian rock consists primarily of chemical sediments, volcanoclastic rocks, turbidite related wackes, as well as argillitic rocks (Leube et al., 1990). They have undergone metamorphism to meta-graywackes, shales, phyllites, tuffs, and schists. According to Asihene and Barning (1975), the metasediment series was divided into 5 fold divisions of arenaceous and argillaceous units (Table 2.1); whereas the meta-volcanics was divided into 3 main volcanic units (Table 2.2) (Kesse, 1985).

The metavolcanic Birimian rock is formed by andesitic and basaltic lavas, which have undergone metamorphism to greenstones, hornblende-actinolite-schist, calcareous chlorite-schists and amphibolites (Kesse, 1985). Currently, there are three divisions of meta-volcanic birimian (Table 2.2).

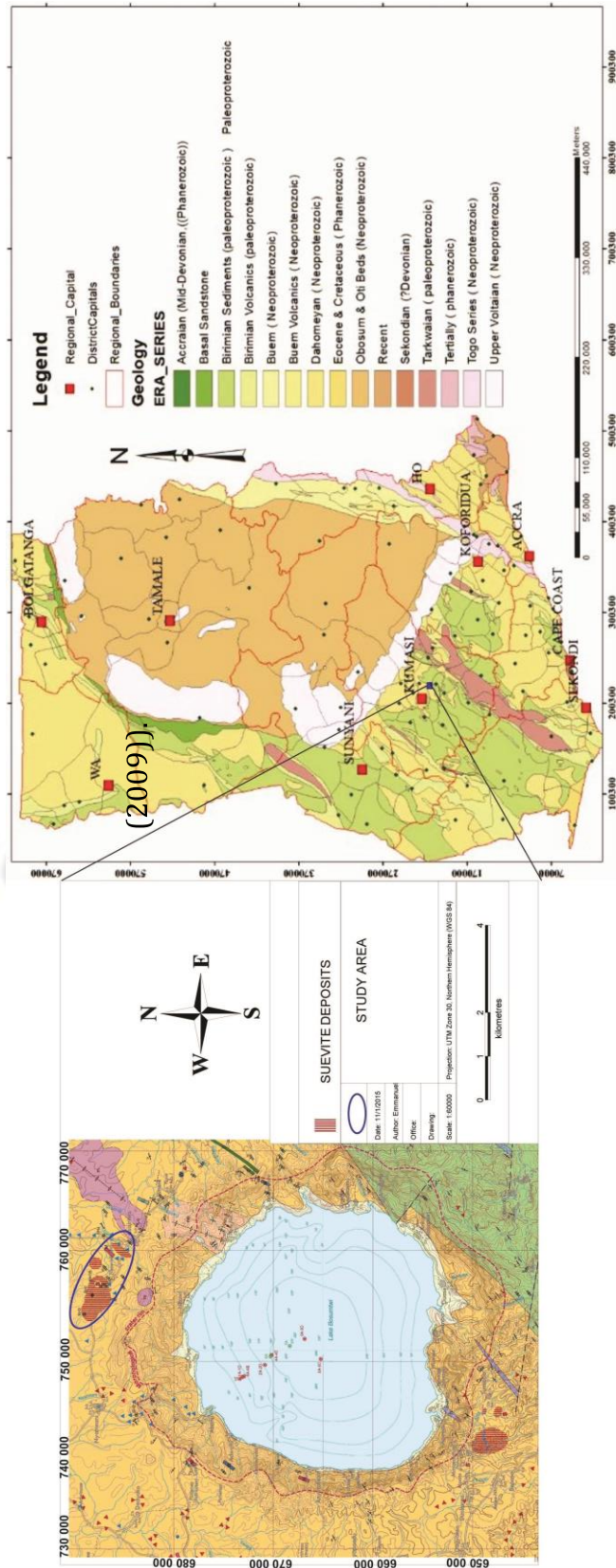


Figure Location of study area relative to geological map of Ghana (adapted from Duodu (2009)).

Table 2.1: Division of the metasedimentary Birimian, (adapted from (Asihene and Barning, 1975)).

SUBSERIES	COMPOSITES LITHOLOGY
-----------	----------------------

Upper Arenaceous	Yellowish brown to buff, massive metasandstones, metagreywackes and metasiltstone.
Upper Argillaceous	Yellowish brown to ochre coloured rock, a set of phyllite, siltstone and their tuffaceous varieties
Mid Arenaceous	Black, grey and dark grey phyllite interbedded with greenish grey and buff coloured tuffaceous phyllite
Lower Argillaceous	Black, grey and dark grey phyllite interbedded with greenish grey and buff coloured tuffaceous phyllite
Lower Arenaceous	Lithic assemblage of meta-greywacke, metasandstone, metasiltstone, phyllite and tuffaceous varieties of these rock types.

Table 2.2: Divisions of the Meta-volcanic Birimian (adapted from (Asihene and Barning, 1975)).

Basic volcanics	Consists of the meta-volcanic Birimian and is then further divided into greenstones (metabasalt and metadolerite), amphibolite greenstones and actinolite-chlorite greenschists
Acid volcanics	Makes up Meta-rhyolites, quartz feldspar porphyry, felsites and quartz-chlorite-schists.
Sedimentary volcanics	Consists of Meta-tuffaceous greywacke, quartzites, and schistose conglomerate

According to Kesse (1985), the Birimian of Ghana has six volcanic belts; namely *Kibi-Winneba, Ashanti, Sefwi, Bui, Bole-Navrongo, and Lawra* belts. The volcanic belts and sedimentary basins are intruded by three types of granitoids differing in age, mineralogy and chemistry (Rae, 2009; Leube et al., 1990). The **Granitoids** is the general term used to refer simultaneously to a range of intermediate (quartz diorite, granodiorite, plagiogranite) to felsic (true granites and a variety

of other felsic types) intrusives. In addition, the current general terms used to represent the Birimian volcanic belts (Dixcove-type) and Sedimentary basins (Cape Coast-type) granitoids are simply “**belt**” and “**basin**” granitoids (Rae, 2009).

Basin granitoids are therefore, dominated by two-mica granites. These granitoids are well foliated, potash rich granitoids. They are characterized by the presence of many enclaves of schists and gneisses. Cape Coast type granites are generally associated with Birimian metasediments. The mineralogical composition of these granitoids are quartz, muscovite, biotite, microcline, tourmaline, albite, almandine, beryl, spessartite and Kaolin (Ferriere et al., 2007).

Belt granitoids; these granitoids are dominated by hornblende granites or granodiorite, grading into quartz diorite and hornblende diorite. Type granite forms non-foliated discordant and semi-discordant bodies in the enclosing country rocks. These granitoids are generally associated with Birimian metavolcanics. The Dixcove has lower SiO_2 and Al_2O_3 but slightly higher CaO content than the Cape Coast granite. And then it has higher Na_2O/K_2O ratio (Ferriere et al., 2007).

The late K-rich granitoids (Post Tarkwaian) are also termed as the Bongo, Tongo and Bonso granitoids. These granitoids are dominated by the mineralogical minerals such as hornblende, microcline and plutonic. They are younger than the Dixcove granite (Junner, 1940; Kesse, 1985).

2.1.3 The Tarkwaian System

The scattered group of supracrustals which originated from shallow water sediments are known as Tarkwaian after the town of Tarkwa in southern Ghana, where they are gold bearing. The Tarkwaian supracrustals contain the Birimian fragments but are less deformed and metamorphosed than the Birimian. It is found in all Birimian Supergroup Belts (Junner, 1940). After the radiometric dating

done by Eisenlohr and Hirdes (1992) on the detrital material of Tarkwaian sediments, they found that age range falls within 2190 to 2130 Ma; which coincides with the Birimian System.

There are four main divisions of the Tarkwaian that are provided by Junner (1940); and is summarized in Table 2.3. The Banket is important series because it contains the gold in several places.

Table 2.3: Division of Tarkwaian (adapted from (Junner, 1940)).

Series	Thickness(m)	Composite in lithology
Huni Sandstone	1370	Sandstones, grits and quartzites with bands of phyllites
Tarkwa Phyllites	120 – 400	Huni sandstone transitional beds and green, greenish grey chloritic, sericitic phyllites and schists
Banket series	120 – 160	Tarkwa Phyllite transitional beds and sandstones, quartzites, grits, breccias and conglomerates
Kawere	250 – 700	Quartzites, grits phyllites and conglomerates

2.1.4 Volta Basin sediments

When discussing the geology of Ghana, the Volta basin cannot be left out. It covers almost one half of the entire area approximately 100,000 km^2 of the country. The Voltaian basin consists mostly of flat lying or low dipping sediments overlying a major Precambrian unconformity (Rae, 2009).

Currently, the Volta Basin sediments are divided into Lower Bombouaka Supergroup, the Oti (or Penjari) Supergroup and Tamale Supergroup. The lower Bomouaka Supergroup consists of sandstones, a central section of siliceous and clay-rich units. However, the Oti sediments are mainly dominated by a distinctive lower sequence of tillite, sandstones, carbonate and fine grained chery sediments (silexite) (Bertrand-Sarfati et al., 1991; Affaton et al., 1991).

The last sequence of sediments is Tamale supergroup, which is the youngest sequence of sediments in the Volta Basin. Furthermore, it consists of a basal section of sediments that include glacial tillites. These are also overlain mostly by crossbedded quartz sandstones with subordinate shale and mudstones (Affaton et al., 1991; Rae, 2009).

2.2 Local geology

2.2.1 Geology of the survey site

Introduction

The geological stratigraphy around lake Bosumtwi (study area) consists of series of supracrustal rock types; namely meta-sedimentary as well as meta-volcanic rock, belonging to the range 2.1 to 2.2 Ga Birimian Supergroup. Detritus from this sequence is formed by overlying Tarkwaian Supergroup. These supergroups are intruded by mostly granitoides (Jones et al., 1981).

Paleoproterozoic supracrustals

Birimian rocks

The Bosumtwi impact event excavated in lower greenschist facies metasediments of the 2.1 to 2.2 Ga Birimian Supergroup (Jones et al., 1981; Leube et al., 1990). The lithology of country rocks that constituted the target rocks, are chiefly made of meta-graywackes, shales, and phyllite of the proterozoic Birimian Supergroup and some intrusion of granitoides (Junner, 1940; Ferriere et al., 2007).

There are three types of impact breccias which appear at and around the crater. There are monomict lithic breccia, polymict lithic breccia and also suevites. The suevites however, occur locally in the north as well as southwest of the crater (Reimold et al., 1998; Boamah and Koeberl, 2003). In this research, the suevites dominate the geology of the study area in the northern part of lake Bosumtwi (Figure 2.2). Greywackes are the most dominant clast types in many suevite samples in the survey area.

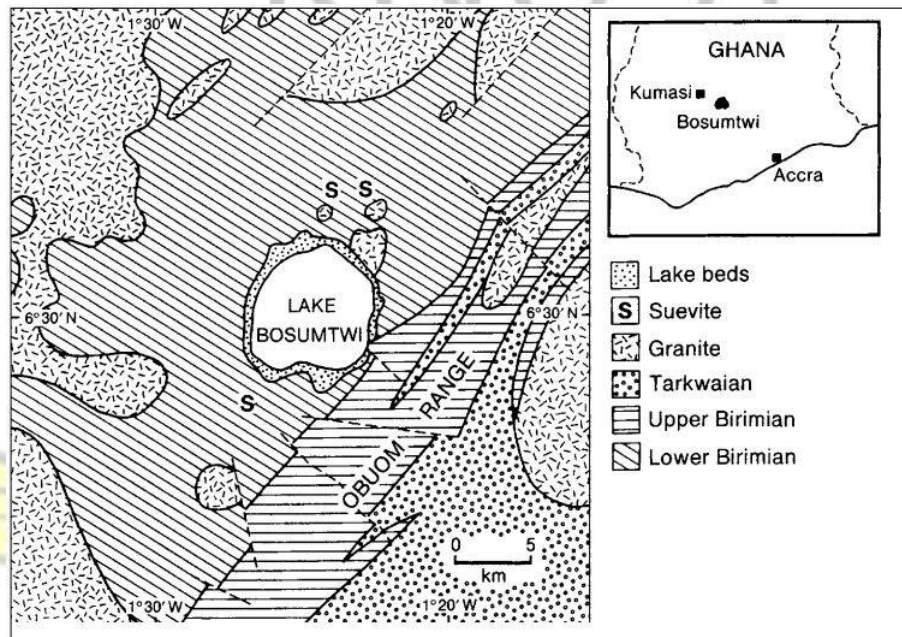


Figure 2.2: Simplified geological map of the Bosumtwi impact structure (Jones et al., 1981; Koeberl et al., 1998; Reimold et al., 1998).

Greywackes appear in many lithological varieties between silty, tuffaceous phyllite and tuffaceous grits. They are fine to coarse-grained, light to dark grey, impure fragmental arenaceous rocks containing a mixture of clastic and tuffaceous rocks. The finer types exhibit good cleavage, but the coarser ones are more massive, and it is not easy to identify the cleavage (Woodfield, 1966). The coarse grained types grade into pebbly grits and conglomerates, and the fine grained types into phyllites. In addition, the coarser types particularly contain a high proportion of feldspar; and the greywackes found in the road cut are highly fractured and shattered.

With regards to the phyllites, they are grey to black, fine grained rocks that are usually argillaceous but are tuffaceous in some places. The Birimian metasediments have a general NE-SW strike and steep dips approximately 80° to either NW or SE. However, in the vicinity of the crater there are irregularities in strikes and dips, and these irregularities are believed to have been caused by the impact event due to the crater (Moon and Mason, 1967).

Intrusive bodies

There are many Proterozoic granitic intrusions in the region around the crater (Junner, 1940; Woodfield, 1966). Among them are highly weathered and fractured granitic dikes as well, like those that were found when the new road was cut from Asisiriwa towards Boamadumasi. Then, other granites outcrops include foliated types by small dikes of aplite and quartz veins. In addition, most of granitic dikes conform to the foliations or bedding planes of the Birimian rocks into which they are penetrated as well. The Pepiakese granite complex to the northeast of the crater is formed of a range of rock types, namely hornblende diorite, biotite, muscovite granite, and almost pure albite rock (Jones, 1985; Reimold et al., 1998).

Impact breccia

Geological surveys have been carried out in the past to map the breccia exposures around the crater (Junner, 1940; Woodfield, 1966; Reimold et al., 1998). However, we cannot say that all breccia represent impact breccia because Reimold et al. (1998) had said that at least some of the breccias are likely as a result of lateralization and secondary mass-wasting process in this tropical and topographical environment where weathering can attain thicknesses in excess of 50 m. Depending on the composition and texture, the breccia at Bosumtwi might be grouped into three categories such as an autochthonous monomict breccia, a probably allochthonous polymict lithic breccia as well as suevite breccias (Koeberl et al., 1998).

An excellent example of consolidated breccia was recently found along the road cut from Asisiriwa to Boamadumasi. Furthermore, the monomictic breccia types have occurred along the road from Nyamiani to Asisirwa and along the crater as well. Moon and Mason (1967) have described this rock as shattered rocks and as having formed by changes of the surface elevation without much lateral displacement.

Suevites

The suevites are the most interesting deposit which was mapped using integrated geophysical methods in this research. The Bosumtwi suevites are similar to the suevites of the Ries crater in Germany. The suevite deposits occur in the north and southwest of the Bosumtwi crater, and it was first mentioned by (Junner, 1940).

Stoßfler and Grieve (1994) have defined suevites as polymictic clastic matrix breccia containing glass fragments, rock and mineral clasts exhibiting various stages of shock metamorphism. The Bosumtwi suevites are greyish in colour with abundant glass and clasts. They represent a type of ejecta materials that contain target lithology in all degrees of shock metamorphism. The northern Bosumtwi suevites are situated within $1^{\circ}23.5'$ to $1^{\circ}24.5'W$ and $6^{\circ}33.2'$ to $6^{\circ}34.2'N$ about 2.5 km from the lakeshore outside of the rim, (figure 2.1 and 2.2). It occurs as large blocks and as patchy massive deposits which are often covered by thick vegetation and cocoa trees in the area around 1.5 km^2 . The large suevite outcrops contain melt inclusions as well as rock fragments (greywacke, shale, granite, phyllite). The matrix of suevite is formed by fine grained particles of many quartz, feldspar, and vesicular glass as well (Littler et al., 1961; Chao, 1968; Boamah and Koeberl, 2003; Ferriere et al., 2007).

Boamah and Koeberl (2003) have done significant study of the geology and geochemistry of suevite samples of this area. Thus, the stratigraphic column of BH1 and BH3 (figure 2.3) revealed that the thicknesses of suevites range between 1.5 – 15 m and 2 -10 m respectively.

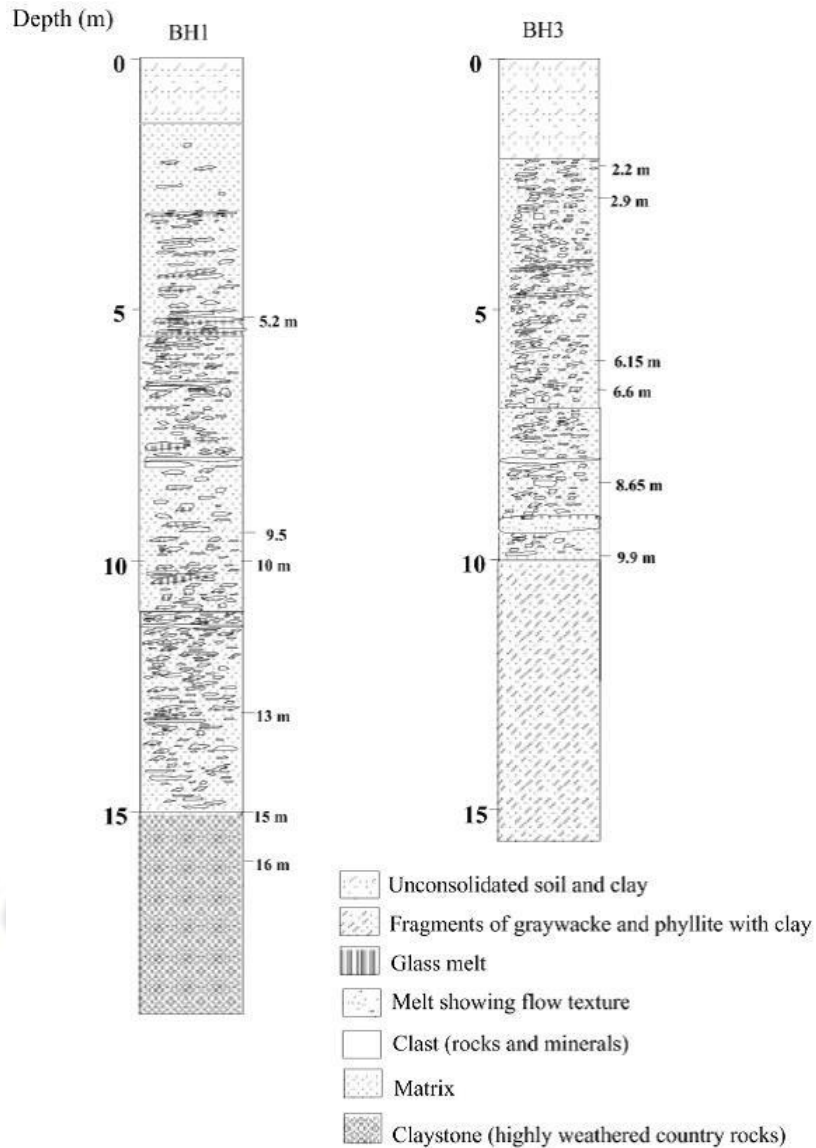


Figure 2.3: Stratigraphic column for 2 drill holes through suevites (Boamah and Koeberl, 2003).

Chapter 3

THEORETICAL BACKGROUND

3.1 The seismic refraction method

3.1.1 Introduction

Seismic surveying was first carried out in the early 1920s for environmental and engineering purposes. A seismic survey can provide a clear and detailed picture of subsurface geology (Kearey et al., 2009). The seismic refraction surveying

method uses seismic energy that returns to the Earth's surface after traveling through the ground, and are detected by seismic wave detectors called Geophones. It can be undertaken at three different scales: global (using earthquake waves), crustal (using explosion), and near-surface for engineering applications(using a sledge hammer, drop weight) (Reynolds, 2011). For the purpose of this thesis, emphasis is placed on the near-surface investigations.

The major strength of the seismic refraction method is to determine the depth and lateral extents of layers, thicknesses and volume of deposits (Kearey et al., 2009). The most commonly computed geophysical parameter is the seismic velocity of the layers present; and it is used to determine the rock properties. Seismic refraction is increasingly being used in hydrogeological investigations to determine saturated aquifer thickness, weathered fault zones etc. It has also a major importance in the location of faults and joints. The method is also used for the mapping of near-surface sedimentary layers, the location of the water table whereas in an engineering application, it is used for investigating the foundation conditions including the determination of depth to bedrock (Reynolds, 2011).

3.1.2 Main assumption and limitations of the seismic refraction method

The general assumptions relating to the seismic refraction method are that the subsurface is composed of series of layers, separated by planar or dipping interfaces. Also, within each layer seismic velocities were assumed to be constant; and that the velocity increases with depth. Furthermore, the acoustic impedance contrast for different layers must be very large. In order to detect the first arrivals in seismic refraction survey, a layer must a) be underlain by a layer of higher velocity, and b) have enough thickness and velocity such that the produced head waves become first arrivals on the surface, otherwise it can give rise to the problem of hidden layer and blind zone (Kearey et al., 2009).

3.1.3 Seismic waves

The Earth rings like a bell when a short term forces, caused by either natural or artificial sources of deformational energy are applied. The ground motions produced by the energy sources within the Earth involve a small elastic deformation or strain; in response of internal forces in the rocks, or stresses. A body subjected to stress undergoes a change of shape and/or size known as strain. Up to a certain limiting value of stress, known as yielding strength of a material, the deformation (strain) is directly proportional to the applied stress (Hookes'Law). And therefore, a medium suffers lateral as well as longitudinal strain . The ratio of the lateral to the longitudinal strain is known as poisson's ratio (σ) which describes the compressibility of the medium (Kearey et al., 2009; Barton, 2007). The deformation of the medium depends on its material properties, which are known as elastic moduli. The Young's modulus(E), Bulk modulus(K), and Shear modulus(μ) are the elastic moduli of rocks and are given by equations: 3.1, 3.2 and 3.3 respectively.

$$E = \frac{\frac{F}{A}}{\frac{\Delta L}{L}} \quad (3.1)$$

$$K = \frac{P}{\frac{\Delta V}{V}} \quad (3.2)$$

$$\mu = \frac{\tau}{\tan\theta} \quad (3.3)$$

where;

$\frac{F}{A}$: longitudinal stress

$\frac{\Delta L}{L}$: longitudinal strain

$\frac{\Delta V}{V}$: volume strain

$\tan\theta$: shear strain; finally

P : volume stress
(Pressure)

t : is time

When stress varies with time within the materials, strain varies simultaneously; therefore, the balance between stress and strain results in seismic waves. Milsom (2003) has defined the seismic wave as an acoustic energy transmitted by the vibration of materials particles in the ground. The seismic wave is divided into two types, namely body waves and surface waves (Kearey et al., 2009). The acoustic wave equation in 2D medium, with varying properties is given by equation 3.4.

$$\frac{\partial^2 P}{\partial t^2} = c^2(x, z) \left[\frac{\partial^2 P}{\partial x^2} + \frac{\partial^2 P}{\partial z^2} \right] \quad (3.4)$$

where; P is wave
pressure c is wave
speed x is horizontal
distance z is depth.

3.1.4 Body waves

Body waves are subdivided into two types: Compressional wave and Shear wave. Compressional waves are the pressure waves that propagate in all media (solids and fluids) with highest velocity of any possible wave motions. They are also known as Longitudinal, Primary or P-Waves. The Shear waves usually come after the P-waves; and their movement causes particles to vibrate at right angles to the direction of wave propagation (which can only happen in solid medium). Alternatively, these are called transverse, Secondary or S-wave. Also, because shear modulus (μ) is zero in fluids, S-waves do not propagate through fluids (Kearey et al., 2009).

According to Kearey et al. (2009) and Telford et al. (1990), in an homogeneous and isotropic medium, the propagation velocities of seismic pulses are determined by elastic moduli and the densities (ρ) of materials through which they pass. The seismic waves propagate with different velocities in different

geological materials. It depends on many factors such as: minerals content, lithology, porosity, pore fluid saturation, degree of fracturing, pore pressure, and to some extent temperature. Therefore, the velocities of P-waves and S-waves are respectively given by:

$$V_p = \sqrt{\frac{K + \frac{4}{3}\mu}{\rho}} \quad (3.5)$$

$$V_s = \sqrt{\frac{\mu}{\rho}} \quad (3.6)$$

Furthermore, the ratio of these velocities in any given material, is determined solely by the value of poisson's ratio for that material.

$$\frac{V_p}{V_s} = \sqrt{\frac{2(1 - \sigma)}{1 - 2\sigma}} \quad (3.7)$$

From equation 3.6 and 3.7, it seems that the P and S wave velocities decrease with density, but it is not so. Shear and bulk moduli both, increase more quickly as a function of density, so strictly speaking P and S wave velocities increase with density (Telford et al., 1990). Table 3.1 adopted from Reynolds (2011), shows the P-wave velocities of some Earth's materials.

3.1.5 Ray path of seismic refracted wave

When P-wave is incident at an oblique interface across which a contrast in acoustic impedance exists, four types of waves are generated: reflected and transmitted Pwaves, reflected and transmitted S-waves (Figure 3.1). Since the energy of a wave is proportional to the amplitude square, the information of energy partition into the reflected and refracted body waves at normal incidence in a given material is expressed by Zoeppritz's equation 3.8 (Telford et al., 1990).

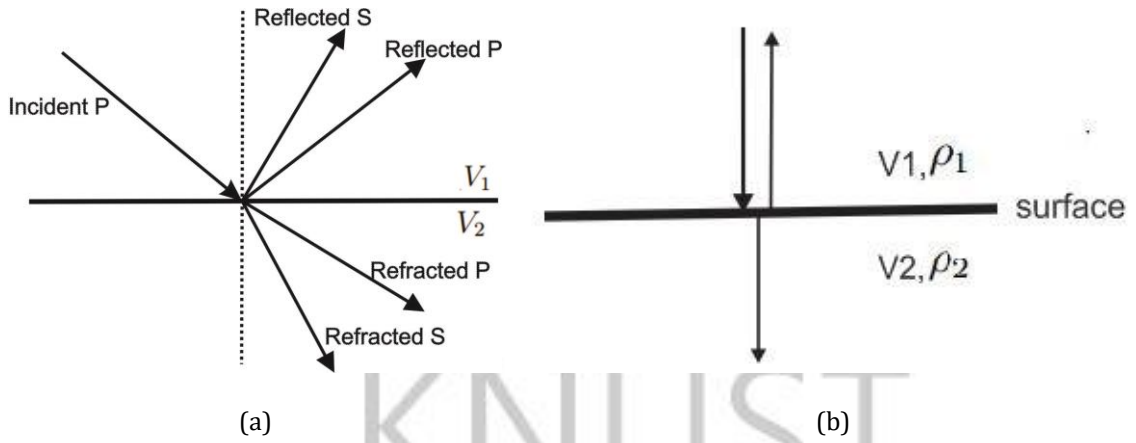


Figure 3.1: Reflection and refraction of (a) obliquely incident ray and (b) normal incident ray adapted from Telford et al. (1990)

$$R = \frac{A_1}{A_0} = \frac{\rho_2 V_2 - \rho_1 V_1}{\rho_2 V_2 + \rho_1 V_1} = \frac{Z_2 - Z_1}{Z_2 + Z_1} \quad (3.8)$$

Where ρ_1 , V_1 , Z_1 and ρ_2 , V_2 , Z_2 are density, P-wave velocity and acoustic impedance values of the first and second layers respectively.

$$T = \frac{A_2}{A_0} = \frac{2Z_1}{Z_2 + Z_1} \quad (3.9)$$

A_0 , A_1 and A_2 are the amplitudes of the incident, the reflected and transmitted rays respectively. Where R and T stand for reflection and transmission coefficients respectively. R varies from -1 to +1. A negative value of R means a phase change of π or 180° in reflected ray. When there is no acoustic impedance contrast across an interface, even if the density and velocity values are different in two layers $Z_1=Z_2$; all incident energy is transmitted ($R=0$). However, if $R = +1$ or $R = -1$, all the incident energy is reflected.

The principle of seismic refraction is based on Huygens's and Fermat principles and Snell's law of refraction (Befus, 2010). The seismic refraction method respects the Fermat's principle in such a way that the ray path representing the seismic wave propagation in the ground is always considered as minimum path. As seismic waves travel from a layer (or medium) of low seismic velocity into a

layer (or medium) of higher seismic velocity, some are refracted toward the lower velocity layer, and others are reflected back into the first layer. According to Snell's law, the ratio of the angle of incidence (i) to the angle of refraction (r) is equal to the ratio of velocity of layer 1 to the velocity of layer 2 (equation 3.10). At the critical angle (equation 3.11), most of the seismic energy is transmitted along the surface of the second layer with seismic wave velocity of the second layer. When a seismic energy is propagating in the medium, it obeys the Huygens's principle where every point on an advancing wavefront can be regarded as the source of a new energy wave. Then, as this energy propagates along the surface of contact, it generates new energy wave in the upper layer (or medium) known as head wave (Reynolds, 2011; Haeni, 1986).

Table 3.1: Examples of P-waves velocities (Reynolds, 2011).

Materials	V_p (m/s)
Air	330
Water	1450 – 1530
Petroleum	1330 – 1400
Loess	300 – 600
Soil	100 – 500
Solid glacier	3000 – 4000
Glacial moraine	1500 – 2700
Sand (loose)	200 – 2000
Sand (dry,loose)	200 – 1000
Sand (water saturated,loose)	1500 – 2000
Sand and gravel (near surface)	400 – 2300
Sand and gravel (at 2km depth)	3000 – 3500

Clay	1000 – 2500
Estuarine muds/clay	300 –1800
Sandstone	1400 – 4500
Limestone (soft)	1700 – 4200
Limestone (hard)	2800 – 7000
Dolomites	2500 – 6500
Rock salt	4000 – 5500
Shales	2000 – 4100
Granites	4600 – 6200
Basalts	5500 – 6500
Sulphides ores	3950 – 6700
Pulverised fuel ash	600 – 1000
Landfill refuse	400 – 750
Concrete	3000 – 3500
Disturbed soil	180 – 335
Clay landfill (compacted)	355 – 380

The head waves arrive at the Earth's surface where they can be detected by the geophones as is shown on figure 3.2. Geophones generate and send electrical signals to a seismograph. From a series of geophones placed on the ground, the seismic arrival time versus the shot to detector distance can be plotted to give a time distance curve (figure 3.3). The head wave eventually overtakes the direct wave, despite the long travel path and reaches the surface first.

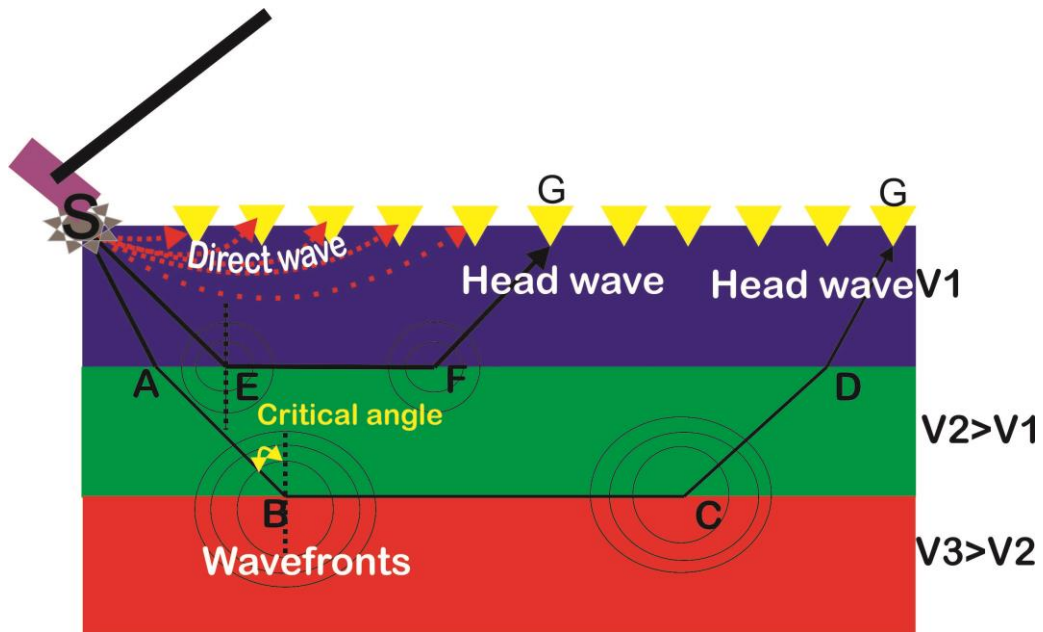


Figure 3.2: Simplified cartoon example of seismic refraction. Propagation of the waves according to Huygens's principle.

By analysis of the travel-time curve for refracted rays it is possible to calculate the depth to the underlying layer. The first arrival of seismic energy on a surface is either a direct wave or refracted wave. The direct wave is overtaken by a refracted wave at the crossover distance and beyond this distance the first arrival is always a refracted wave (head wave).

At a critical distance the reflected arrival is coincident with the first critically refracted arrival and the travel times of the two are identical. The critical distance is thus the offset at which the reflection angle equals the critical angle (Reynolds, 2011). Figure 3.3 shows the travel time for 3 horizontal layers.

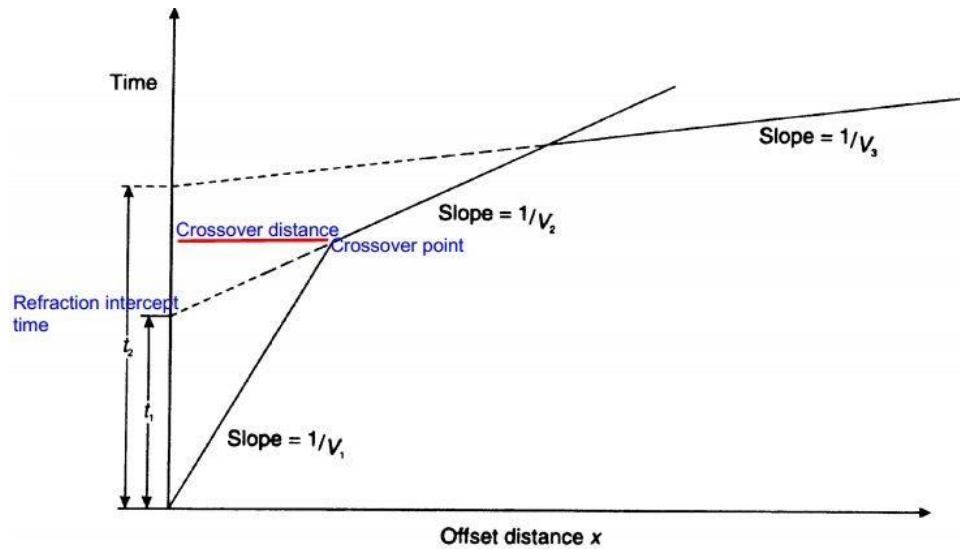


Figure 3.3: Travel time distance curves for 3 horizontal layers; modified from Reynolds (2011).

$$\frac{\sin(i)}{\sin(r)} = \frac{V_1}{V_2} \quad (3.10)$$

$$i_c = \sin^{-1}\left(\frac{V_1}{V_2}\right) \quad (3.11)$$

By analysis of the travel-time curve for refracted rays (Figure 3.2 it is possible to calculate the thicknesses of underlying layers (equations 3.12 to 3.17) (Reynolds, 2011).

For two layers case

Travel time is given by:

$$T = T_{SE} + T_{EF} + T_{FG} = \frac{X}{V_2} + \frac{2Z_1\sqrt{V_2^2 - V_1^2}}{V_2V_1} \quad (3.12)$$

Using the intercept time (t_1) of first layer, its thickness is given by

$$Z_1 = \frac{t_1V_1}{2\cos(i_c)} = \frac{t_1V_1V_2}{2\sqrt{V_2^2 - V_1^2}} \quad (3.13)$$

For three layers case

Travel time is given by:

$$T = T_{SA} + T_{AB} + T_{BC} + T_{CD} + T_{DG} = \frac{X}{V_3} + \frac{2Z_1\sqrt{V_3^2 - V_1^2}}{V_3V_1} + \frac{2Z_2\sqrt{V_3^2 - V_2^2}}{V_3V_2} \quad (3.14)$$

By considering the intercept time (t_2) of the second layer, its thickness is given by

$$Z_2 = \frac{t_2V_2V_3}{2\sqrt{V_3^2 - V_1^2}} - \frac{Z_1V_2\sqrt{V_3^2 - V_1^2}}{V_1\sqrt{V_3^2 - V_2^2}} \quad (3.15)$$

For n layers

Travel time is given by:

$$T = \frac{X}{V_n} + \frac{2Z_1\sqrt{V_n^2 - V_1^2}}{V_nV_1} + \frac{2Z_2\sqrt{V_n^2 - V_2^2}}{V_nV_2} + \dots \quad (3.16)$$

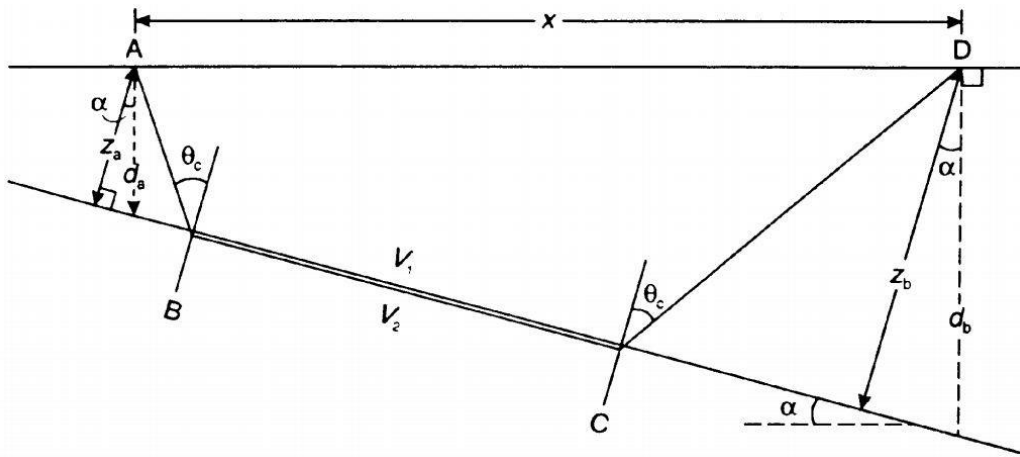
Generally, when $V_n > V_{n-1}$ the thickness of n-1 layer is calculated by

$$Z_{n-1} = \frac{t_{n-1}V_{n-1}V_n}{2\sqrt{V_n^2 - V_{n-2}^2}} - \frac{Z_{n-2}V_{n-1}\sqrt{V_n^2 - V_{n-2}^2}}{V_{n-2}\sqrt{V_n^2 - V_{n-1}^2}} \quad (3.17)$$

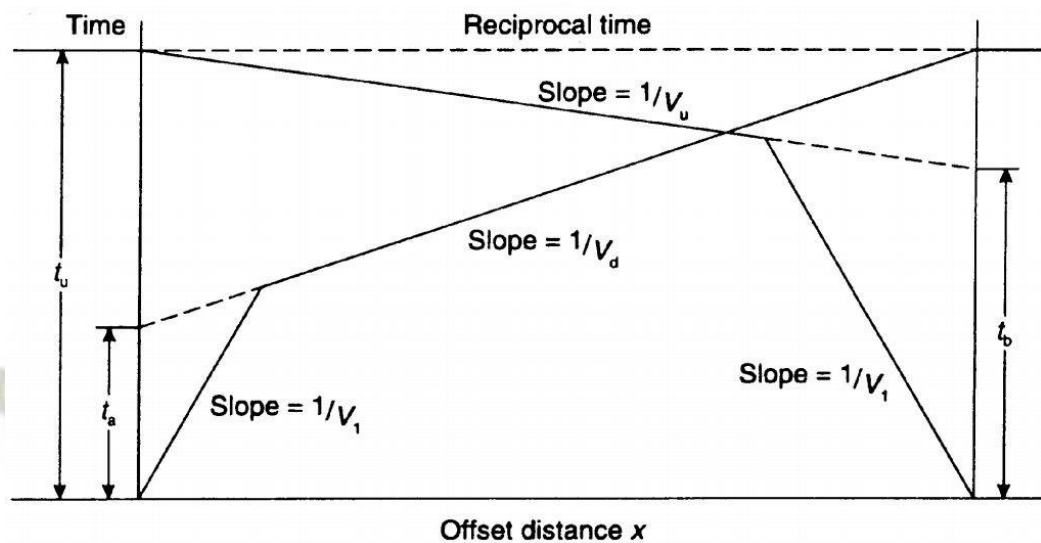
where, V_n and V_{n-1} are the velocity values of lower and upper layers respectively.

3.1.6 Dipping layer

For dipping refractors, the travel time curves are asymmetrical. Furthermore, the inverse of slope of travel time curve doesn't give the "true layer velocity" but it represents apparent velocity. In up dip shot, the apparent velocity is greater than true velocity; whereas during the down dip shot the apparent velocity is less than true velocity. For instance in figure 3.4a, a point D is located down dip from point A. Therefore, it is advisable to carry out both forward (down-dip) and reverse (up-dip) shots in order to determine the layer velocity as well as refractor geometry.



(a)



(b)

Figure 3.4: (a) Raypath geometry over a refractor dipping at angle(α) and (b) travel time-distance graph for forward and reverse shooting directions, (Reynolds, 2011)

For the dipping refractor, the total travel time of head wave is given by:

$$T_{ABCD} = \frac{x \cos(\alpha)}{V_2} + \frac{[(Z_a + Z_b) \cos(\theta_c)]}{V_1} \quad (3.18)$$

In equation 3.18, Z_a and Z_b are the distances perpendicular to the refractor for up and down dips respectively; they are computed by equation 3.19(a) and (b).

$$Z_a = \frac{t_a V_1}{2 \cos \theta_c} \quad (3.19a)$$

$$Z_b = \frac{t_b V_1}{2 \cos(\theta_c)} \quad (3.19b)$$

For the dipping interface with angle of dip (α), the apparent velocities V_u and V_d for up dip and down dip respectively are calculated by equations 3.20(a) and (b) where θ_c is critical angle.

$$V_u = \frac{V_1}{\sin(\theta_c - \alpha)} \quad (3.20a)$$

$$V_d = \frac{V_1}{\sin(\theta_c + \alpha)} \quad (3.20b)$$

Therefore, the depths d_a and d_b to the layer up dip and down dip respectively are given by equations 3.21(a) and (b).

$$d_a = \frac{Z_a}{\cos(\alpha)} = \frac{V_1 t_a}{2 \cos(\theta_c) \cos(\alpha)} \quad (3.21a)$$

$$d_b = \frac{Z_b}{\cos \alpha} = \frac{V_1 t_b}{2 \cos(\theta_c) \cos(\alpha)} \quad (3.21b)$$

where the angle of dip is calculated by

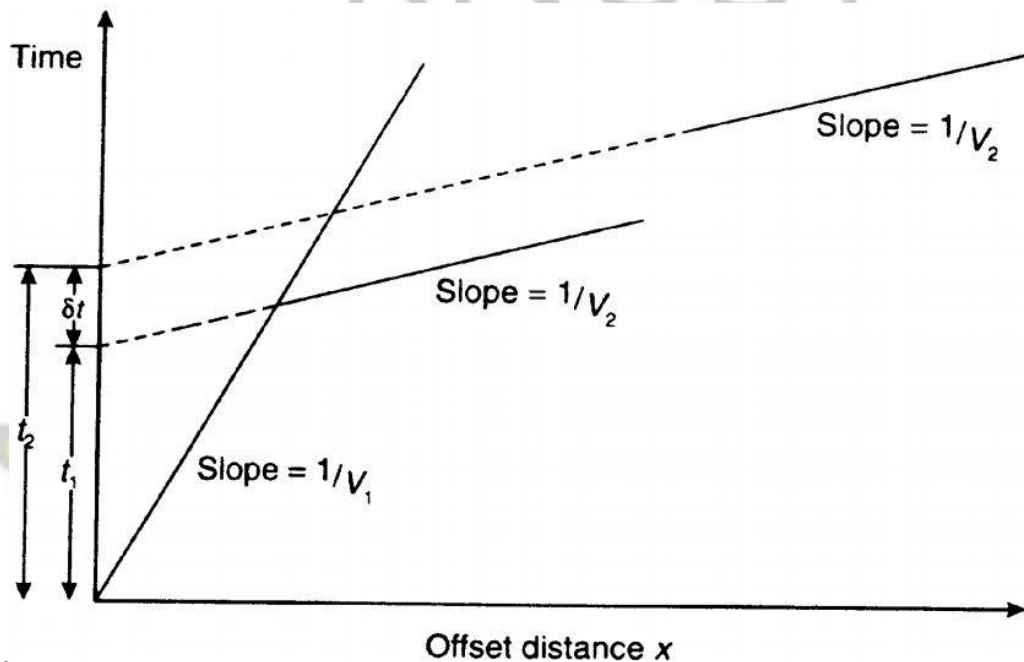
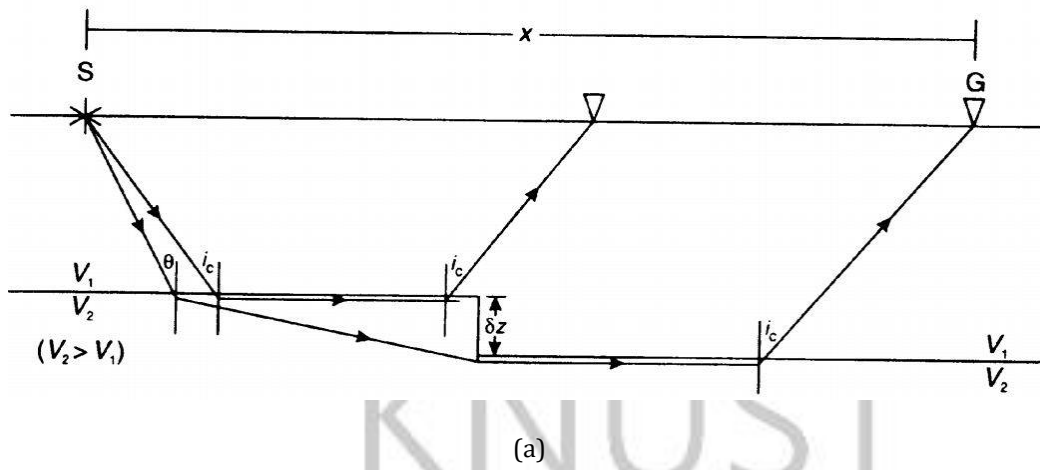
$$\alpha = \frac{1}{2} \left[\sin^{-1} \left(\frac{V_1}{V_d} \right) - \sin^{-1} \left(\frac{V_1}{V_u} \right) \right] \quad (3.22)$$

Finally, from Everett (2013) for small angle of dip $\alpha < 10^\circ$ such that $\cos^2(\alpha) \approx 1$.

$$V_2 = \frac{V_d + V_u}{2} \quad (3.23)$$

3.1.7 Discontinuity layer

So far the boundary has been assumed as planar interface and continuous. However, if the boundary is faulted, then there will be a sharp offset in the travel time-distance graph (figure 3.5)



(b)

Figure 3.5: (a) Raypath geometry over a boundary with a step discontinuity but no lateral change in velocity and (b) the travel time-distance graph (Reynolds, 2011).

When the size of the step discontinuity is small compared to the depth to the boundary, equation 3.24 is used to estimate the difference in depth (δz) to the boundary (refractor). While the delay time (δt) can be measured from travel time-distance graph.

$$\delta z = \frac{\delta t V_1 V_2}{\sqrt{V_2^2 - V_1^2}} \quad (3.24)$$

3.2 The resistivity method

3.2.1 Introduction

Electrical resistivity survey is one of electrical methods used to determine the spatial resistivity distribution (or its reciprocal-conductivity) in the ground. Electrical resistivity techniques have been used since the early 1900s by Frank Wenner and the Schlumberger brothers (Loke and Lane Jr, 2004; Kearey et al., 2009). The electrical resistivity technique is used in archeology, environmental, hydrology investigation and engineering applications as well (Loke, 1999; Reynolds, 2011; Aning et al., 2013a).

3.2.2 Basic dc resistivity principles

In direct current resistivity methods, a direct or low frequency (0.1-30 Hz) alternating current is introduced to the ground through current electrodes (C_1, C_2); and the resulting potential differences are measured on the Earth's surface by two other potential electrodes (P_1, P_2) (Kearey et al., 2009; Reynolds, 2011).

Since the subsurface is mostly heterogeneous, when electric current is introduced to the ground it follows the path of least resistance concentrating in the area of conductive material and avoiding the area of resistive material. For instance, as shown in figure 3.6, the blue geological formation is more conductive than the orange formation. Therefore, the deviation from the pattern of potential differences expected from the homogeneous ground provide information on the form and electrical resistivity of subsurface heterogeneities (Griffiths and Barker, 1993).

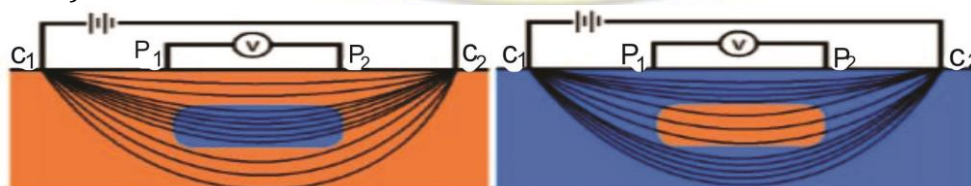


Figure 3.6: Variations in electric current density due to the variation in subsurface resistivity (Griffiths and Barker, 1993).

The electrical resistivity survey is based on Ohm's law which controls the flow of electric current in a conducting medium, and is sensitive to resistivity contrast of the subsurface (Reynolds, 2011; Everett, 2013). In order to estimate the subsur-

face resistivity it is necessary to consider the subsurface current density (\vec{J}) and its electric field (\vec{E}), which are related by Ohm's law 3.25a:

$$\vec{J} = \sigma \vec{E} \quad (3.25a)$$

$$\vec{E} = \frac{\vec{J}}{\sigma} = \rho \vec{J} \quad (3.25b)$$

Let's consider a single current electrode planted at a point of spherical coordinates system, and returning electrode at infinity figure 3.7. The current will spread out symmetrically in all 3 dimensions. Hence the current density is given by equation 3.26; where the numerator represents the magnitude and direction of current, and denominator stands for the area of the sphere of radius (r).

$$\vec{J} = \frac{I\hat{r}}{4\pi r^2} \quad (3.26)$$

The corresponding electrical potential at point P, is expressed as

$$V_r = \int_r^\infty E dr = \frac{I\rho}{4\pi r^2} dr = \frac{I\rho}{4\pi r} \quad (3.27)$$

Since the electrical current cannot flow through the non conducting air, the surface area of a halfspace, $2\pi r^2$ is always considered. The electrical potential is therefore reduced to

$$V_r = \frac{I\rho}{2\pi r} \quad (3.28)$$

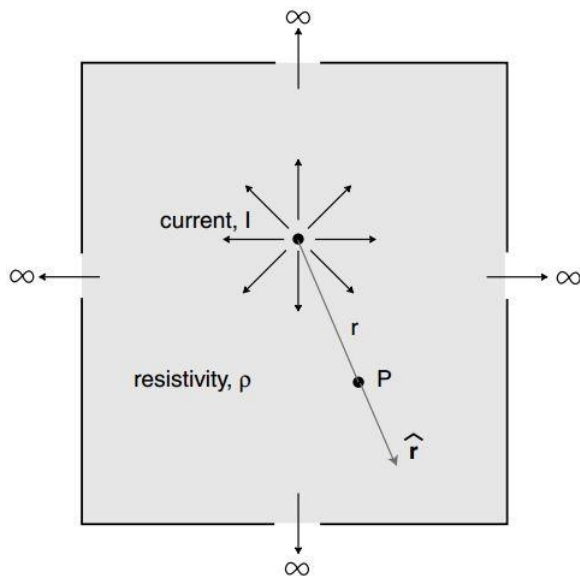


Figure 3.7: Current injection into a wholespace of uniform resistivity from Everett (2013).

If, however, a current sink (+) and return (-) electrodes (C_1, C_2) are planted at fixed distance relative to potential electrodes (P_1, P_2) as shown in figure 3.8, a new potential distribution occurs. Electrical potential at potential electrode (P_1) is given by $V_{P1} = V_{C1} + V_{C2}$.

$$V_{P1} = \frac{\rho I}{2\pi} \left(\frac{1}{r_1} - \frac{1}{r_2} \right) \quad (3.29)$$

Similarly,

$$V_{P2} = \frac{\rho I}{2\pi} \left(\frac{1}{r_3} - \frac{1}{r_4} \right) \quad (3.30)$$

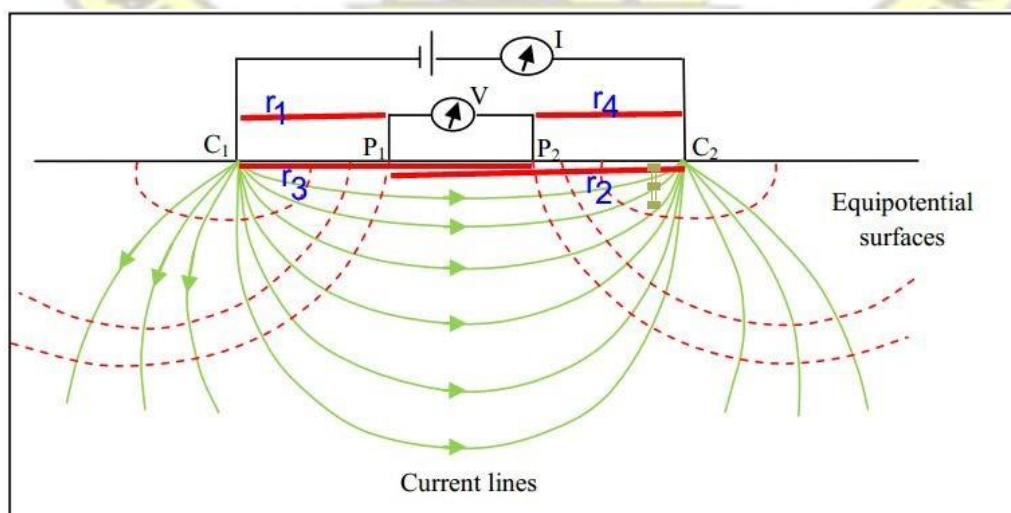


Figure 3.8: Generalized form of electrode configuration in resistivity surveys modified from, Knaflitz et al. (2007).

Therefore, the potential difference between electrodes P_1 and P_2 which is measured on the field is given by:

$$\Delta V = V_{P_1} - V_{P_2} = \frac{\rho I}{2\pi} \left(\frac{1}{r_1} - \frac{1}{r_2} - \frac{1}{r_3} + \frac{1}{r_4} \right) \quad (3.31)$$

Finally, the apparent resistivity (equation 3.32) measured on the field is obtained from equation 3.31, where K is a geometrical factor which takes into account the geometric spread of potential and current electrodes (Reynolds, 2011).

$$\rho_a = k \frac{\Delta V}{I} \quad (3.32)$$

$$k = 2\pi \left(\frac{1}{r_1} - \frac{1}{r_2} - \frac{1}{r_3} + \frac{1}{r_4} \right)^{-1} \quad (3.33)$$

When the subsurface is homogeneous, the resistivity computed from equation 3.32 is “true resistivity” and should be constant and independent of both electrode separation and surface location. However, if the subsurface is heterogeneous then the resistivity will vary with the relative positions of electrodes. In this case, any computed value is different from the true resistivity and is then known as “apparent resistivity” (Kearey et al., 2009). The apparent resistivity is the value obtained as the product of a measured resistance (R) and a geometric factor (K) for a given electrode configuration (Reynolds, 2011).

3.2.3 The geology and resistivity

Electrical resistivity (ρ) (also known as specific electrical resistance) is an intrinsic physical property of a material indicating how strongly it opposes the flow of electric current. It is measured in Ohm-meter (Ωm). Its reciprocal is

electrical conductivity (σ); which indicates how a material conducts the current. This is expressed in Siemens per meter(S/m) (Reynolds, 2011).

The subsurface resistivity is related to various geological parameters such as conductivity of minerals, fluid content, porosity, degree of water saturation in the rock, temperature of the water, and dissolved electrolytes (Loke, 1999; Telford et al., 1990; Reynolds, 2011).

Indeed, Archie et al. (1942) developed an empirical formula as shown in equation 3.34, for the effective resistivity of a rock formation (ρ) which takes into account the porosity(Φ), the volume fraction (S) of the pores containing water, and the resistivity of the water (ρ_w) which can depend on the quantity and conductivity of dissolved materials. Archie's Law is used mostly in borehole logging (Reynolds, 2011; Kearey et al., 2009).

$$\rho = a\Phi^{-m}S^{-n}\rho_w \quad (3.34)$$

where a, m and n are empirical constants and lie in the range of $0.5 \leq a \leq 2.5$; $1.3 \leq m \leq 2.5$ and $n \approx 2$ respectively (Archie et al., 1942). The knowledge of resistivity values of some subsurface materials is key in mapping the subsurface geological features. Resistivity values of some common minerals, rocks and soil types are listed in table 3.2. Sedimentary rocks, which are usually more porous and have higher water content, normally have lower resistivity values compared to igneous and metamorphic rocks. Unconsolidated sediments generally have even lower resistivity values than sedimentary rocks. The resistivity values are dependent on the porosity as well as clay content. Clay soil normally has a lower resistivity than sandy soils. Moreover, the variation of resistivity of groundwater depends on the concentration and conductivity of dissolved materials (Loke, 1999).

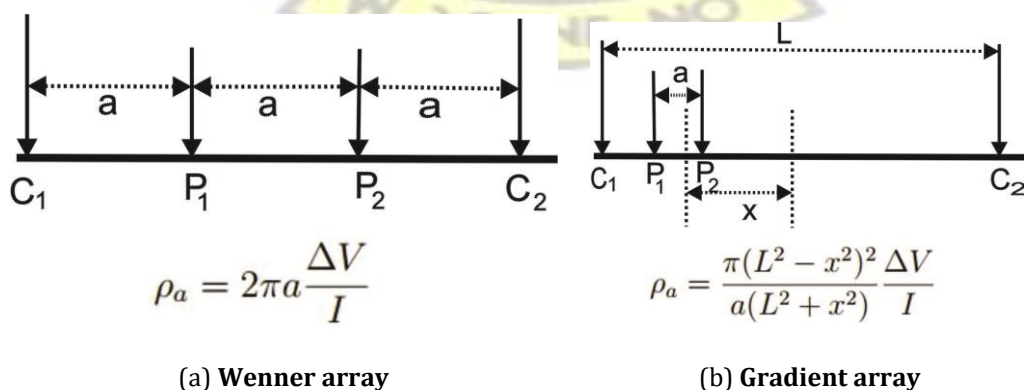
It is evident that for particular minerals and rock types, there is a considerable overlap of resistivity values. This is because the resistivity of particular rock or soil sample depends on many parameters as described above.

Hence, it is not possible solely on the basis of resistivity data to identify all geologic features. As Telford et al. (1990) said “among the physical properties of rocks, and minerals, electrical resistivity shows the greatest variation. Whereas the range in density, elastic wave velocity, is quite small”. That is why, electrical resistivity method could be combined with another geophysical methods such as seismic refraction, Ground Penetrating Radar (GPR) etc, to minimize the problem of ambiguity.

3.2.4 Electrode configuration

The electrodes configurations (arrays) were designed to meet the various resistivity survey objectives. These arrays have different vertical and horizontal resolutions, depth of investigations, horizontal data coverage and signal strengths; as a result of the arrangement as well as separation of current and potential electrodes (Loke, 1999; Loke and Lane Jr, 2004). Each array has therefore particular advantages, disadvantages and sensitivities. Furthermore, the choice of an array for a particular survey depends on sensitivity of the instruments, level of background noise and space available.

Figure 3.9 illustrates the electrode configurations that are mostly used for electrical resistivity surveys and their apparent resistivity formulas. Where, for dipoledipole array n stands for an integer which varies from 1 to 6. The pole-pole array however has the second current and potential electrodes placed at a distance not more than 20 times the separation between the first current and potential electrodes (Wenner, 1912; Loke, 1999; Loke and Lane Jr, 2004; Bernard, 2003; Reynolds, 2011).



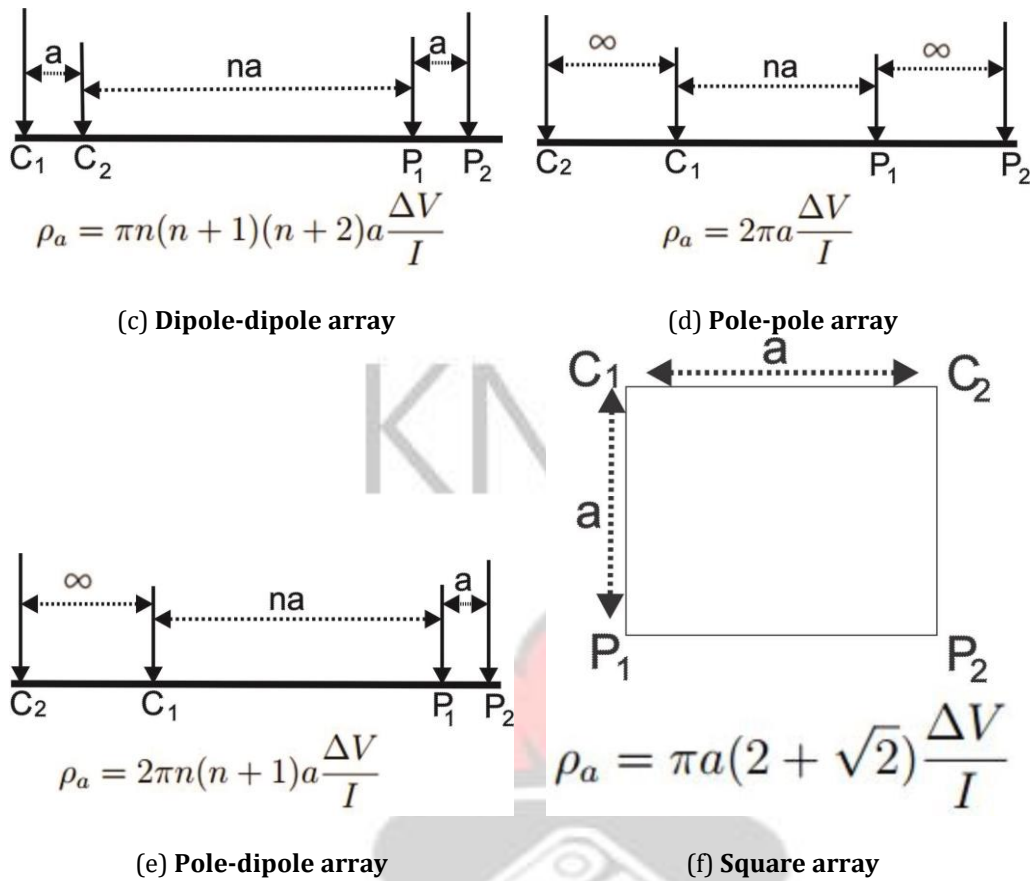


Figure 3.9: Electrode configurations and their apparent resistivity formulas, adapted from Loke (1999) and Reynolds (2011).

Table 3.2: Resistivity values of common geologic materials from Telford et al. (1990) and Reynolds (2011).

Materials	Normal resistivity (Ωm)
Galena	$3 \times 10^{-5} - 3 \times 10^2$
Sphalerite	1.5×10^7
Hematite	$3.5 \times 10^{-3} - 10^7$
Limonite	$10^3 - 10^7$
Magnetite	$5 \times 10^{-5} - 5.7 \times 10^3$
Ilmenite	$10^{-3} - 50$
Quartz	$3 \times 10^2 - 10^6$
Granite	$3 \times 10^2 - 10^6$
Diorite	$10^4 - 10^5$
Basalt	$10 - 1.3 \times 10^7$
Schist(graphite)	$10 - 10^2$
Consolidated Shales	$20 - 2 \times 10^3$

Conglomerates	$2 \times 10^3 - 10^4$
Sandstones	$1 - 7.4 \times 10^8$
Limestones	$50 - 10^7$
Dolomite	$3.5 \times 10^2 - 5 \times 10^3$
Clays	$1 - 10^2$
Alluvium and sand	$10 - 8 \times 10^2$
Moraine	$10 - 5 \times 10^3$
Top soil	$250 - 1.7 \times 10^2$
Clay(very dry)/chalk	50 - 150
Gravel(dry)	1400
Gravel(saturated)	100
Laterite	800 - 1500
Lateritic soil	120 - 750
Dry sandy soil	80 - 1050
sand clay	30 - 225

3.2.5 Depth of current penetration

The depth of investigation in electrical methods depends on two main factors: firstly, the geometry of the cables (type of array, number of electrodes, spacing between electrodes, number of segments) and secondly, the sensitivity of the equipment, the signal to noise ratio, and its ability of filtering the noise through the stacking process. For Schlumberger, Wenner and dipole types of electrode arrays, the maximum depth of investigation is one fifth of the total length of the profile. For pole-pole arrays where one electrode of the current and one electrode of the potential are placed far from the measuring line, the depth of investigation is 0.9 times the length on multi-core cable (Bernard, 2003).

3.2.6 Modes of electrical resistivity surveying

The resistivity surveys are made to satisfy the needs of two distinctly different types of interpretation objectives: 1) the variation of resistivity with depth, shows horizontal stratification of earth materials; and 2) lateral variations in resistivity

that may indicate soil lenses, isolated ore bodies, faults, or cavities (Telford et al., 1990). Traditionally, there are two fundamental modes of electrical resistivity surveying: sounding and profiling.

Vertical electrical sounding (VES)

Vertical electrical sounding also known as vertical profiling or electrical drilling is used especially in the study of horizontal or near horizontal interfaces. In this mode, the center point of the electrode array remains fixed, but the electrodes spacing is systematically increased. As the electrode separation is increased, the current is forced to go deeper into the subsurface and a series of potential differences are measured at different depths. Hence, the information on resistivity variation for different depths at particular fixed central reference point are obtained. The depth of penetration is determined by the array type and nature of each layer.

The results of such a survey are mainly interpreted quantitatively. The measured apparent resistivity values are normally plotted on a log-log graph paper. In this mode, the subsurface resistivity varies solely with depth. The most severe limitation of the resistivity sounding method is that only horizontal (or lateral) changes in the subsurface resistivity are commonly found (Loke and Lane Jr, 2004).

Horizontal profiling

In the electrical resistivity profiling mode, investigation of lateral variation in resistivity is done by moving the array between successive measurements along the survey line while keeping the electrode spacing fixed. After that, the horizontal resistivity variations at specific depth may be investigated by individual measurements made at the points of a grid. It is advisable to carry out first a vertical electrical sounding in order to determine the suitable electrode spacing. The results of such a survey are normally interpreted qualitatively. They can also either be presented in the form of profiles or as a contour map of the

surveyed area; where the depth of investigation remains constant. Wenner and Schlumberger are the most commonly used arrays in both modes of surveying (Loke, 1999).

Computer controlled multielectrodes or Electrical Resistivity Tomography(ERT)

The clear picture of subsurface anomalies usually requires a techniques for determining both lateral and vertical geological features. The two previously discussed survey techniques are capable of detecting either the lateral variation or vertical variation of electrical resistivity. The electrical resistivity tomography is therefore, a suitable survey technique for mapping areas with moderately complex geology (Griffiths and Barker, 1993; Aning et al., 2013a).

The ERT is a multi-electrode system with a constant spacing between adjacent electrodes. However, the separation between the potential and the current electrodes varies depending on the electrodes configuration. In this techniques the sounding and the profiling techniques are integrated to give the information on both the lateral and the vertical extends of the subsurface. It is a suitable method for 2-D or 3-D surveys.

A typical resistivity section for 2D or 3D survey consists of many data points, but a single electrode quadrupole (figure 3.8) measures only one data point. Therefore, in this technique multi-take out cables connects many electrodes to a resistivity meter. The resistivity meter automatically determines the separation and also which electrodes are to be used as current pair and potential pair. The meter measures the apparent resistivity by using a range of different electrode separations and midpoints, a typical example is shown in figure 3.10 (Loke, 1999). The first step is to make all the possible measurements with electrodes spacing (a). The next sequence of measurement with electrodes spacing (2a) is then made after completing the first measurement, etc.

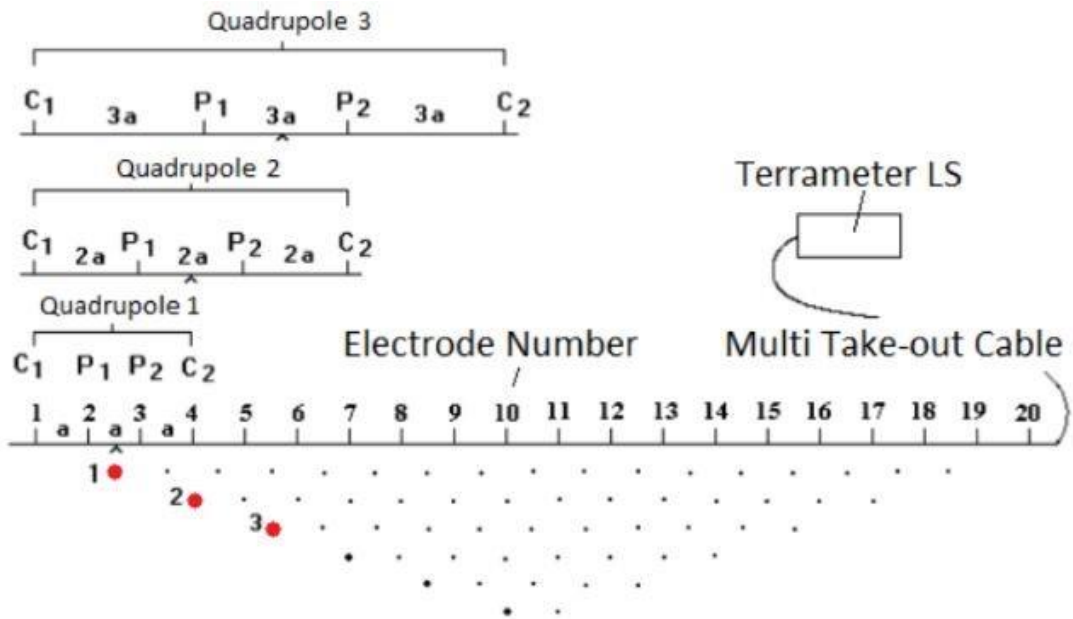


Figure 3.10: 2D resistivity surveys with 3 electrode quadrupole combinations using Wenner array adopted from (Loke and Lane Jr, 2004).

In the case, where the line of prospect is longer than the length of multi-core cable, a technique known as a **roll-along** is used. The roll-along procedure is done by moving the segment of multi-core cable to the end of the cable to enable further measurement, figure 3.11 (Loke, 1999; Bernard, 2003). Measurements for the roll along techniques are normally faster than the first one, because the number of data to be measured are less as a result of data overlap, and only data which do not overlap are measured. The results from ERT surveys, are normally presented in pictorial form using model sections, which give an approximate picture of the subsurface resistivity distribution.

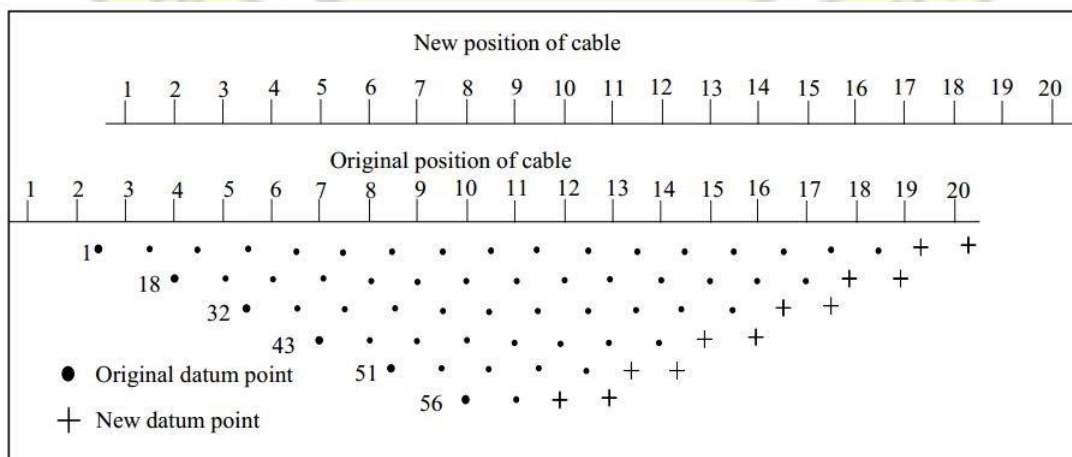


Figure 3.11: The use of the roll-along technique to extend the area covered by a 2-D resistivity survey (Loke and Lane Jr, 2004).

Chapter 4

METHODOLOGY

4.1 Introduction

The main aim of data acquisition is to record the Earth's response to input signal as function of time. The input signal can be either seismic pulse, electromagnetic pulse or electrical current. Thus, a suitable survey technique must be chosen due to main factors such as size of survey area and resolution etc.

The data acquisition was preceded by identification of study area and desk study in order to set the optimum survey design. Seven profiles of lengths varying between 160 and 600 m were located (Figure 4.1). Six of them were specifically in suevitic deposits while one was out side the deposits for cross checking. A preliminary survey was done for three days on two profiles in order to check the credibility of data. Subsequently, the data acquisition was further carried out for 18 days.

4.2 Data acquisition

4.2.1 Seismic refraction survey

In this work, a 6 kg hammer was used as a source of energy to cause vibration of the ground. This non-destructive source was therefore used to deliver 3 consecutive impacts on a rubber plate; where at each shot position the trigger geophone was used to trigger a measurement. 24 geophones of 10 Hz were vertically planted in series into the ground with 4 m spacing, and 8 m shooting interval.

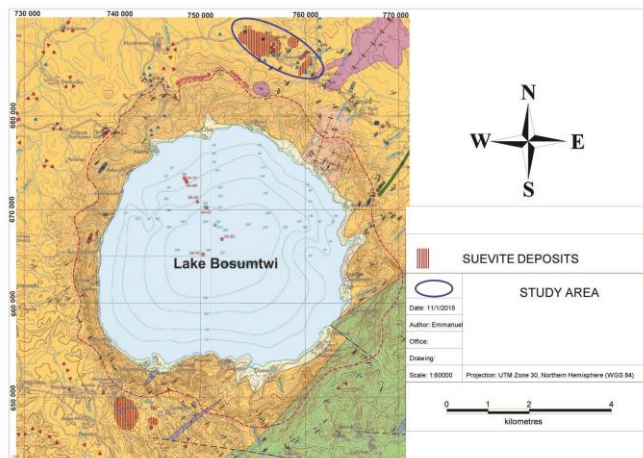
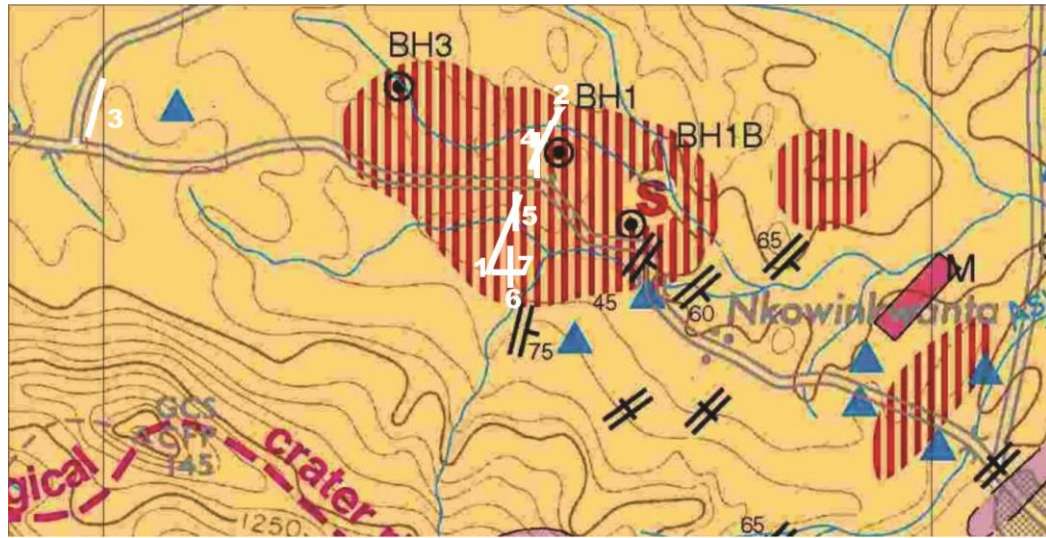


Figure 4.1: Survey design.

Geophones were connected to the cables with jumpers, then directly to the ABEM Tellaroc Mark6 which was powered by 12 V battery (figure 4.2). All profiles were surveyed in this study keeping in mind the topography measurement. During the data collection process, roll along technique was executed to cover 536 m (length of profile). On each section of 96 m, thirteen inline shotpoints and one offset point were considered in order to increase the resolution of seismic refraction tomography.

The roll along technique was implemented by overlapping 2 geophones for the next spread (figure 4.3) in order to increase survey length. Thus, when a

measurement was done at the first station, two spreads as well as 22 geophones were repeatedly removed to the next station. The seismograph was always placed in the center of a spread.

The geophones were placed in-line at constant spacing using a measuring tape. At each station all receivers were tested to ensure that they were functioning properly. During the recording process, three shots were stacked to increase signal to noise ratio. The acquisition parameters for the seismic refraction survey are summarized in Table 4.1.

Table 4.1: List of acquisition parameters.

Profile length	536 m
Number of geophones	25 (one was used as a trigger geophone)
Number of stacking	3
Shot spacing	8 m
Receiver spacing	4 m
offset	4 m

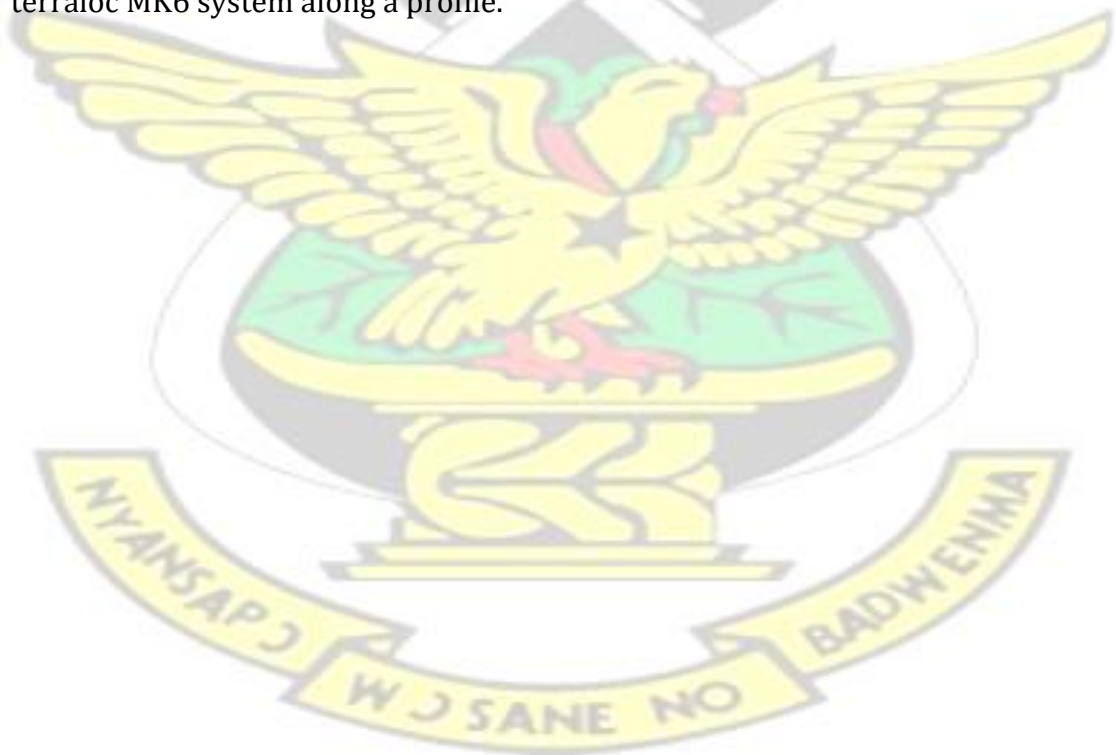


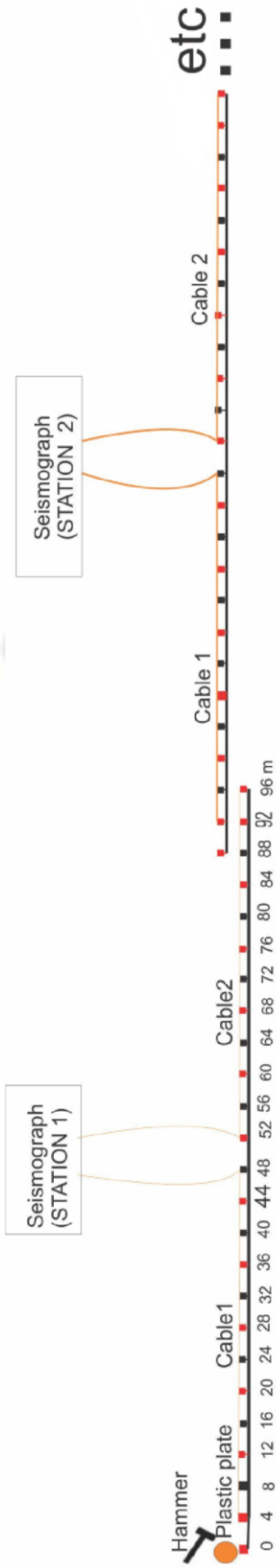
(a)



(b)

Figure 4.2: (a)The set up of Terraloc MK6 System, (b) Data acquisition with the terraloc MK6 system along a profile.





■ Geophone at shot point

■ Geophone

Roll-along technique during seismic refraction survey.

Figure



4.3:

4.2.2 Electrical resistivity survey

During the resistivity survey in this project the ABEM LUND resistivity imaging system was employed for data collection. The ABEM LUND resistivity imaging system is a set of equipment consisting of an electrode selector (ES 10-64C), terrameter SAS 4000, 4 drums of cables, 2 connectors, 84 stainless steel electrodes, 75 electrode jumpers, a 12V car battery and 2 hammers, 0.5 kg each. Figure 4.4 illustrates the entire set up of resistivity imaging system as well as the connection during the measurement. The GPS also was an important tool for locating profiles and indicating topography change along the survey line.

Before setting up the equipment on the survey line, the measuring tape was laid along the line, followed by the planting of electrodes at equal interval of 4 m with the help of hammers. Each cable consists of 21 take-outs with alternating blue (even number) and red (odd number) take-outs; however only the red take-outs were used. Four electrode cables and 41 electrodes were connected with the help of electrode jumpers during the survey. The electrodes were only connected to the odd numbered take-outs (figure 4.5).

The terrameter and selector were connected to the cables at the center of each spread. The 12 V battery was used to power the terrameter and sent current (1000 mA) through the ground, while it was on. After entire connection of the system, the protocols were set at the station. The gradient array and GRAD 4L8 protocol were then selected to enhance the data density, lateral and vertical resolution during the data acquisition (Stummer et al., 2004). It implies that for long layouts 4 potential readings were recorded for single current injection. Before each measurement, the electrode test was done to ensure that the electrodes were properly connected and planted as well. In case an electrode was not working, it was hammered deeper or repositioned or watered until the success of electrode

test.

The computer-controlled multi-electrode system or ERT and roll long survey techniques were combined to scan across the survey line. This allowed the

automatic selection of current and potential electrode pairs during the measurement process.



(a)



(b)



(c)

Figure 4.4: (a and b) Data acquisition with the ABEM LUND imaging system along a profile, (c) elevation measurement with GPS.

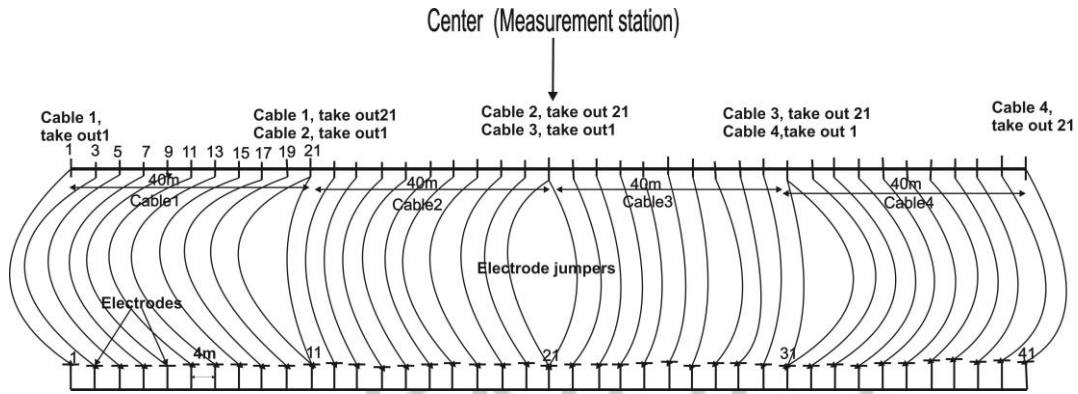


Figure 4.5: Sketch of odd numbered take-outs connection with electrodes.

Since the multi-electrode system was computer controlled; the current was sent at each $(s + 2)(x_N - x_M)$ distance and simultaneously all potential differences between the potential electrode pairs were measured at each midpoint (m).

$$m = \frac{\left(\frac{x_M + x_N}{2}\right) - \left(\frac{x_A + x_B}{2}\right)}{x_N - x_M} \quad (4.1)$$

where s stands for maximum number of potential readings for current injection, while, x_A , x_B , x_M and x_N are the positions of the current and potential electrodes respectively (Dahlin and Zhou, 2006).

The Roll-long technique was employed to cover the profile length of 600 m. Cables were interconnected by connectors, in such a way that a groove must face the cable nearest to the terrameter and selector as well. Each cable covered 40 m; hence, the first spread covered a distance of 160 m. Cable 1 and cable 2 were joined via cable joint, similarly cable 3 and cable 4. At measurement stations, cables 2 and 3 were connected to the instruments.

When all the measurements were done on the first spread, the measuring station was moved by 40 m; and the first cable (cable1) was removed and then connected to cable 4 using a connector. This was done after the measurement on each spread was completed and till the entire length of 600 m was covered. Figure 4.6 illustrates how the roll long technique was implemented, where $c_1, c_2, c_3, \dots, c_{12}$ were the measurement stations.

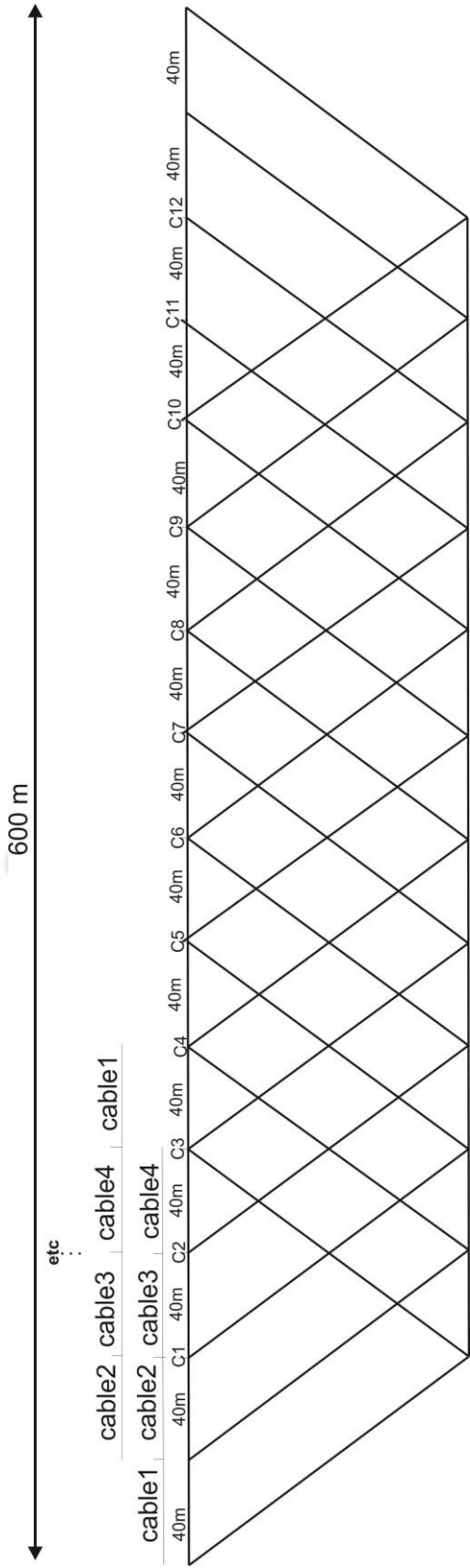


Figure Data acquisition processing roll-along technique.

4.6:

4.3 Data processing

4.3.1 Seismic refraction field data

The seismic raw data was transferred to a computer from the ABEM Terraloc Mark 6. The seismic data was in SG2 format and was processed with the ReflexW software. Data was first imported into the software for 2D data analysis. 2D data analysis was preceded by picking first arrival traveltimes at each first break of seismic pulse (figure 4.7).

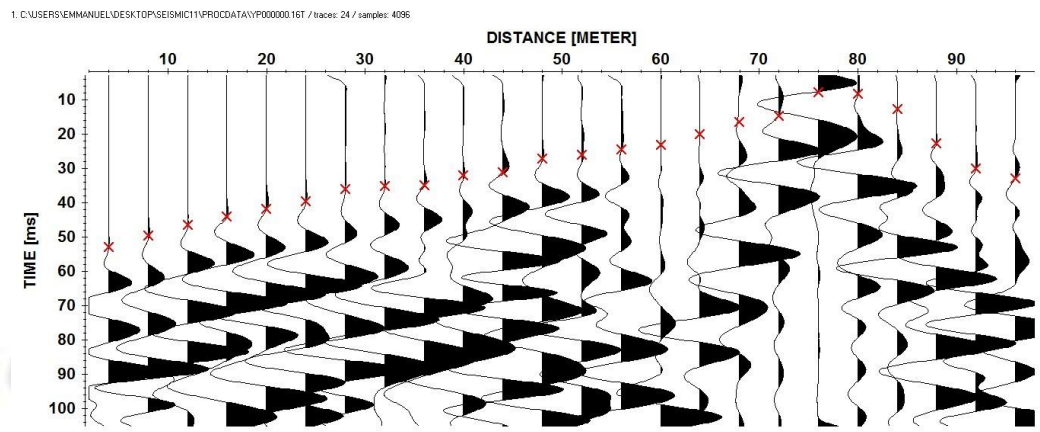


Figure 4.7: First arrival travel time picking.

In travel time analysis, after inserting shot zero travel time of all first arrival seismic traces, layer models were generated. Layer models play an important role in revealing how velocity is changing with depth within the subsurface strata. However, as a result of detailed subsurface image in terms of vertical and lateral velocity gradient tomography models were subsequently generated for every profile.

Seismic refraction tomography also uses first arrival travel times as raw data, and is based on inversion techniques to image the subsurface by considering velocity gradient of 2 dimension pixels. Before the inversion process, maximum velocity variation of 200 % was used in order to enable strong vertical velocity gradient.

Detection of small scale variation was ensured since space increment of 1 m was chosen, while smoothing value in horizontal direction was half the shot spacing (4 m). Finally, 10 iterations were executed as well as topography correction on each 2D velocity model.

4.3.2 Electrical resistivity field data

The raw data obtained during the survey were apparent resistivity. The apparent resistivity values were therefore converted to true resistivity in order to get the subsurface real resistivity distribution. Since the data were acquired in 2D, RES2DINV software was used for the conversion process.

First of all, the raw data were retrieved from the terrameter with the help of Terrameter SAS 4000/SAS 1000 utility software; and then converted to RES2DINV format (.DAT file) to be ready for further processing. After reading the raw data in the RES2DINV environment, the data were edited and bad data points were exterminated (figure 4.8). The bad data points usually appear as spikes, and could be caused by wrong cable connections and poor ground contact of electrodes due to stony or dry ground.

The inversion was then carried out on the edited data. To ensure quality in producing the resistivity model sections with sharp boundaries, the robust inversion was chosen as suitable inversion for the data. Robust inversion is a computer package based on Gauss-Newton least-squares equation, which is given by equation 4.2 (Ellis and Oldenburg, 1994; Loke and Dahlin, 2002).

$$(J^T J + \lambda F_R) \Delta q_k = J^T R_{dg} - \lambda F_R q_k \quad (4.2)$$

Where,

J : Jacobian matrix of current density values

q : The model parameters k : number of

model parameter λ : Damping factor

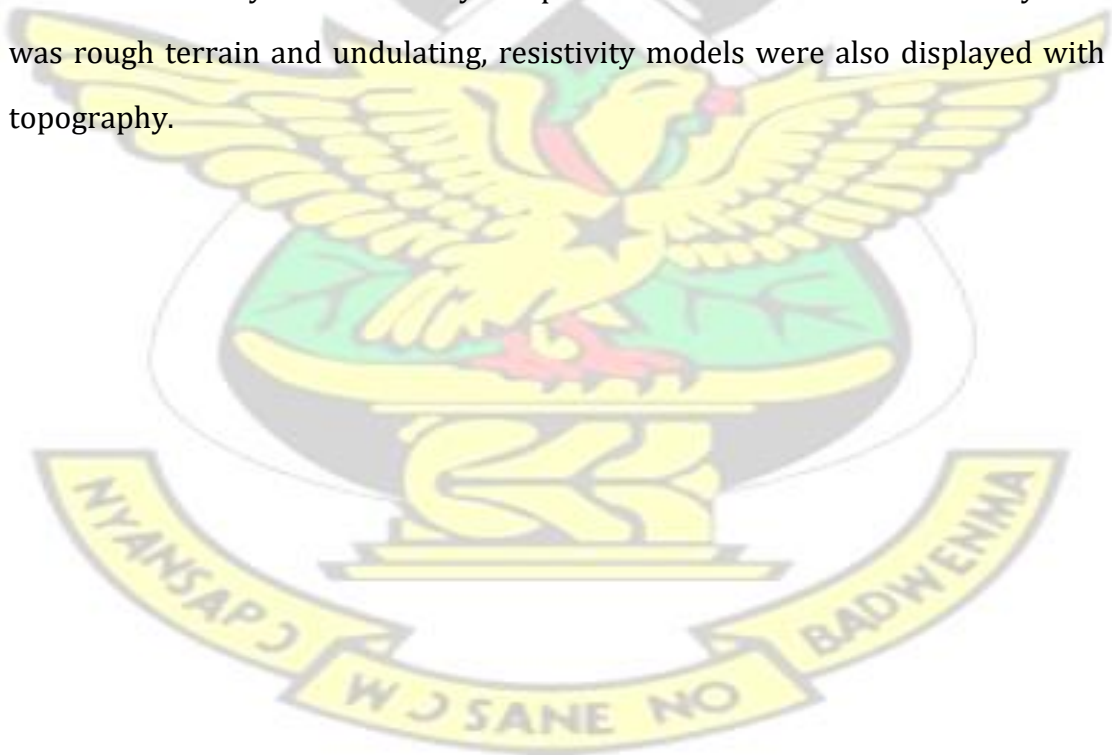
J^T : Transpose of Jacobian matrix

Δq : The model parameter change vector R_d : Weighting matrices g : discrepancy vector (difference between the measured data and the model response)

F_R : Represent a combination of smoothing matrices, weighting matrices, and model roughness vectors in x, y, and z directions.

The details of Gauss-Newton least-squares equation under the inversion process, a reader is kindly refer to the following books:, (Ellis and Oldenburg, 1994; Oldenburg and Li, 1999; Smith et al., 1999; Olayinka and Yaramanci, 2000; Loke and Dahlin, 2002; Auken and Christiansen, 2004).

Under the inversion, the least squares inversion was run so that the true resistivity model section fits the measured data. The pseudosections underwent 5 to 7 iterations to produce model sections with minimal error. The resistivity model sections were subsequently displayed using the user defined logarithmic contour intervals option. As a result; the model sections had the same resistivity values so that they could be easily compared. Since the surface of the study area was rough terrain and undulating, resistivity models were also displayed with topography.



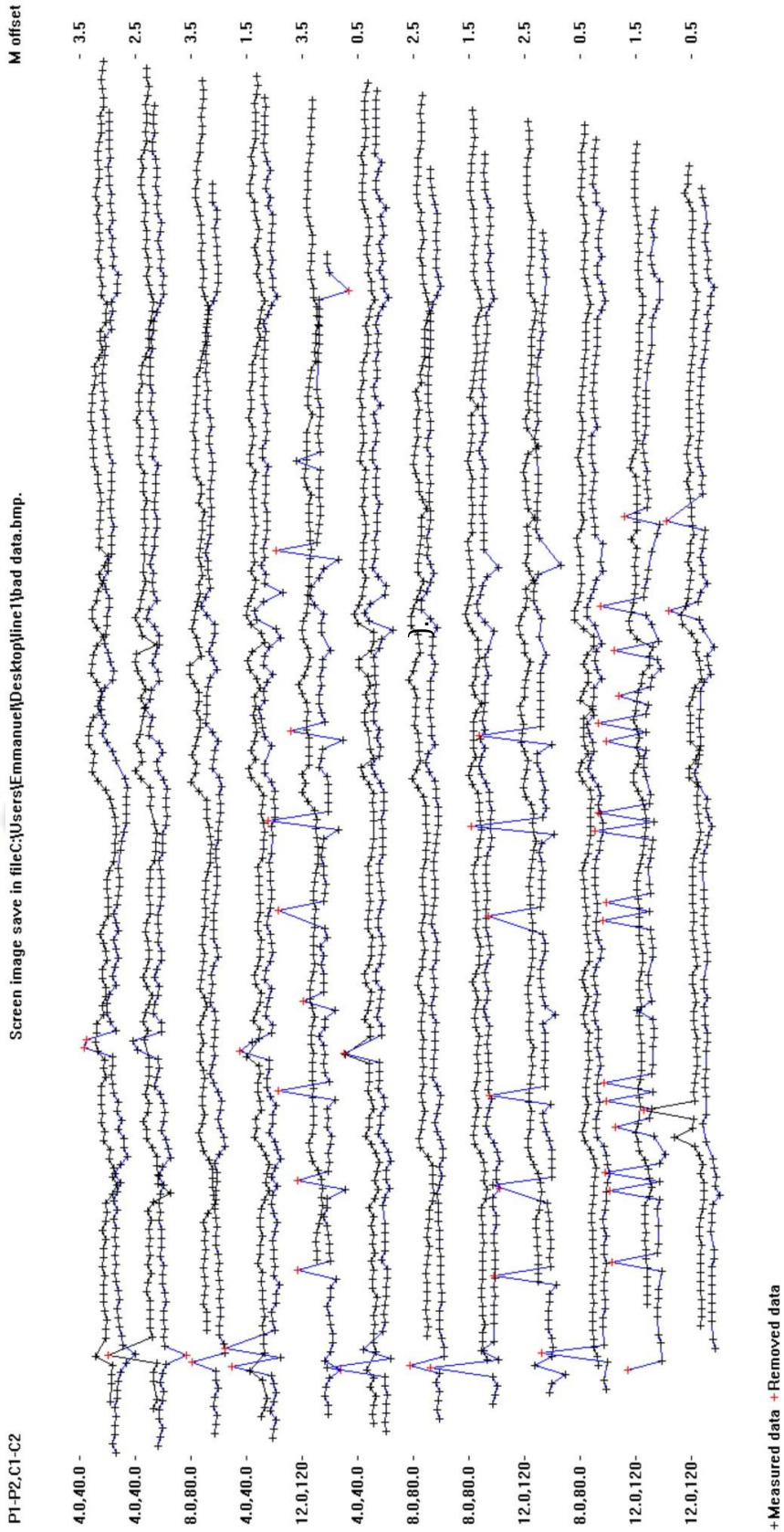


Figure Pseudosection with bad data points (marked with red crosses)

Chapter 5

RESULTS AND DISCUSSIONS

5.1 Introduction

All profiles were geophysically interpreted based on knowledge of the geology of study area (figure 2.3, table 3.1 and table 3.2). The study area is geologically dominated by suevites that have been thrown out during the meteorite impact. Then after, they were gradually overlain by sediments. The suevites are mixture of solidified melted materials. The lithology of suevites has the difference in physical properties with the surrounding materials. In addition to the point based information; electrical resistivity and seismic refraction data were then interpreted together in order to get additional information on lateral extent of suevitic deposits. and subsurface geological units.

Plado et al. (2000) has mentioned that there is a distinctive difference in petrophysical properties between target rocks and impact derived suevites. Thus, suevites have relatively lower resistivity and higher porosity than target rocks. Moreover, the study which was done at Ries impact crater in Germany by Ernstson (1974) has specifically found that resistivities of suevites range from approximately 3 to 50 Ωm . Furthermore, the Chicxulub Scientific Drilling Project (CSDP) indicated ultrasonic P-wave velocity for suevites in Chicxulub impact structure (Mexico) with 25.7% mean porosity and suevites for Chesapeake Bay impact structure (USA) with 9.2% mean porosity ranging between 4.34 and 2.76 km/s and 5.41 and 4.39 km/s respectively (Popov et al., 2014).

5.2 2D resistivity models

The base line for resistivity consisted of two successive profiles separated by 14 m, through which there is the Asisiriwa – Nyameani road. Each profile was 600 m long; figure 5.1 shows a resistivity model section of profile 1 which was surveyed

from North-East to South-West. Electrical resistivity tomography of profile 1 shows that the subsurface is formed by 3 layers. Boundary B delineates the top layer thickness which is less or equal to 4 m and it has slightly high resistivity values from around 60 to 400 Ωm . This layer was interpreted as unconsolidated soil and moist clay. The region just beneath the following locations: 32 to 64 m, 128 to 160 m, 256 to 320 m and 512 to 544 m, with low resistivity distributions could represent the suevites. The resistivities range between 1.56 and 24.00 Ωm , and they occur at depths less or equal to 10 m depth.

The highest resistivities, 6000 – 25000 Ωm , observed at the base may be a zone of bedrock of claystone. Resistivity distribution within the fractured basement rock (claystone) varies laterally; and is as a result of shattering suffered by the basement rocks due to the impact of the suevites. Fractured bedrock zones can be found beyond 10 m deep, at the following locations: 170 to 220 m, 300 to 350 m and 450 to 500 m.

Generally, depending on resistivity distribution within the model section, this profile reveals three layers. A slightly high resistivity top layer, second low resistive layer and a highly resistive third layer. The second layer of thickness ranging between 4 m and 10 m could represent a zone that hosts suevite deposits embedded in moist or clayey soils. It therefore overlay the layer dominated by fractured claystone.

Figure 5.2 is the resistivity image of the second profile. It was surveyed from South-West to North-East. It is subdivided into three layers. The first layer of slightly high resistivity values of 60.00 to 400.00 Ωm represents unconsolidated soil and wet clay.

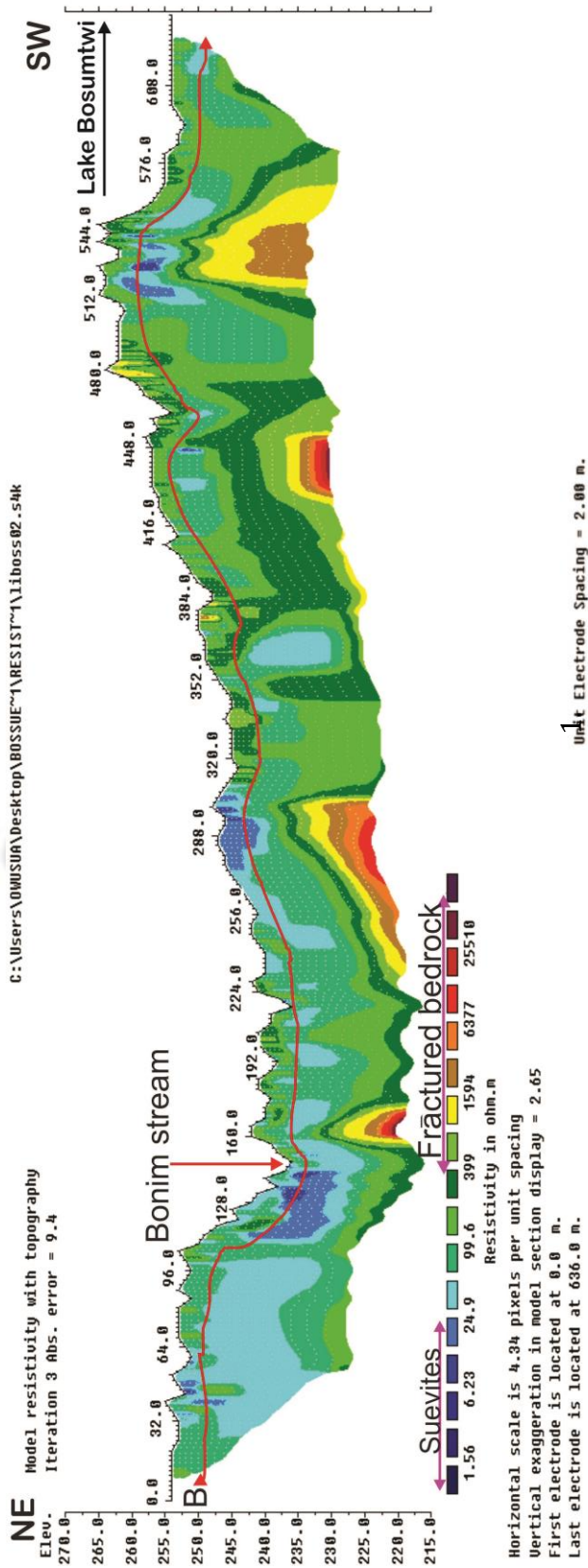
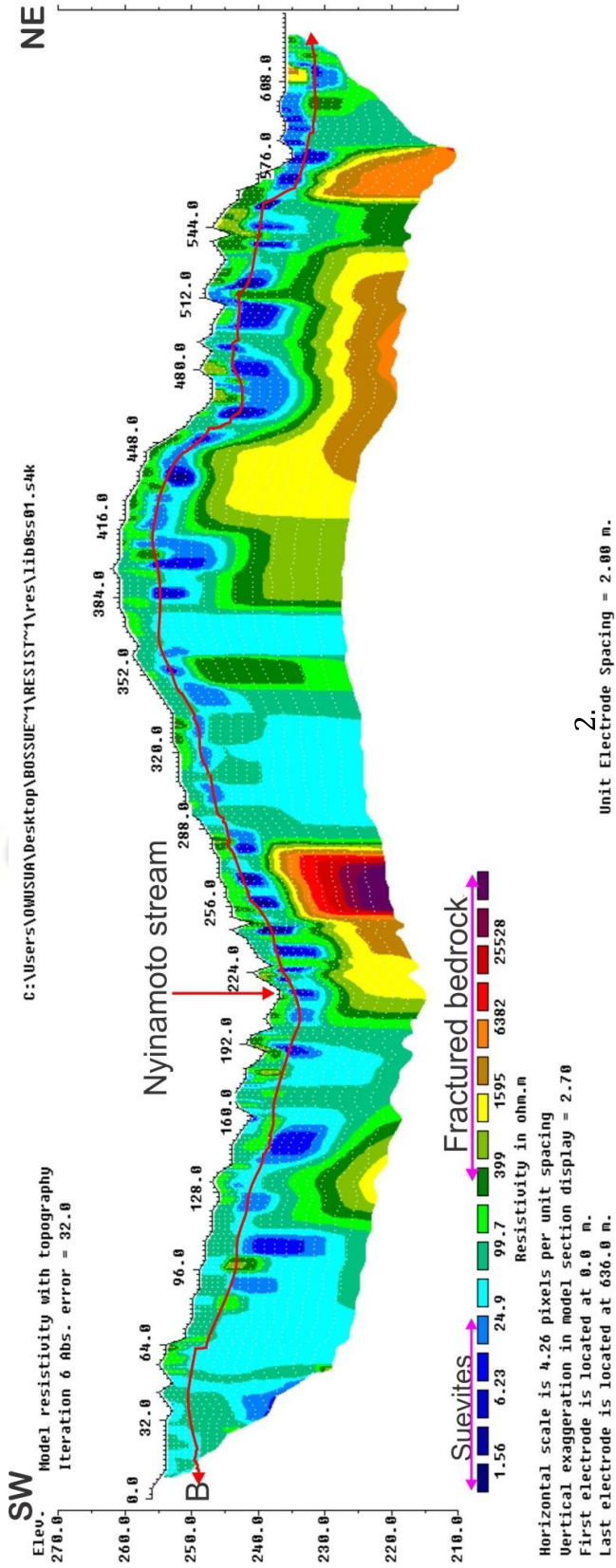


Figure 5.1:2 D resistivity model section of profile

This first layer is delineated by boundary B, where its thickness is less or equal 4 m. It is followed by low resistivity (1.56 to 24.00 Ωm) zones that could stand for second layer dominated by extended suevite deposits. Its thickness varies between 4 and 12 m.

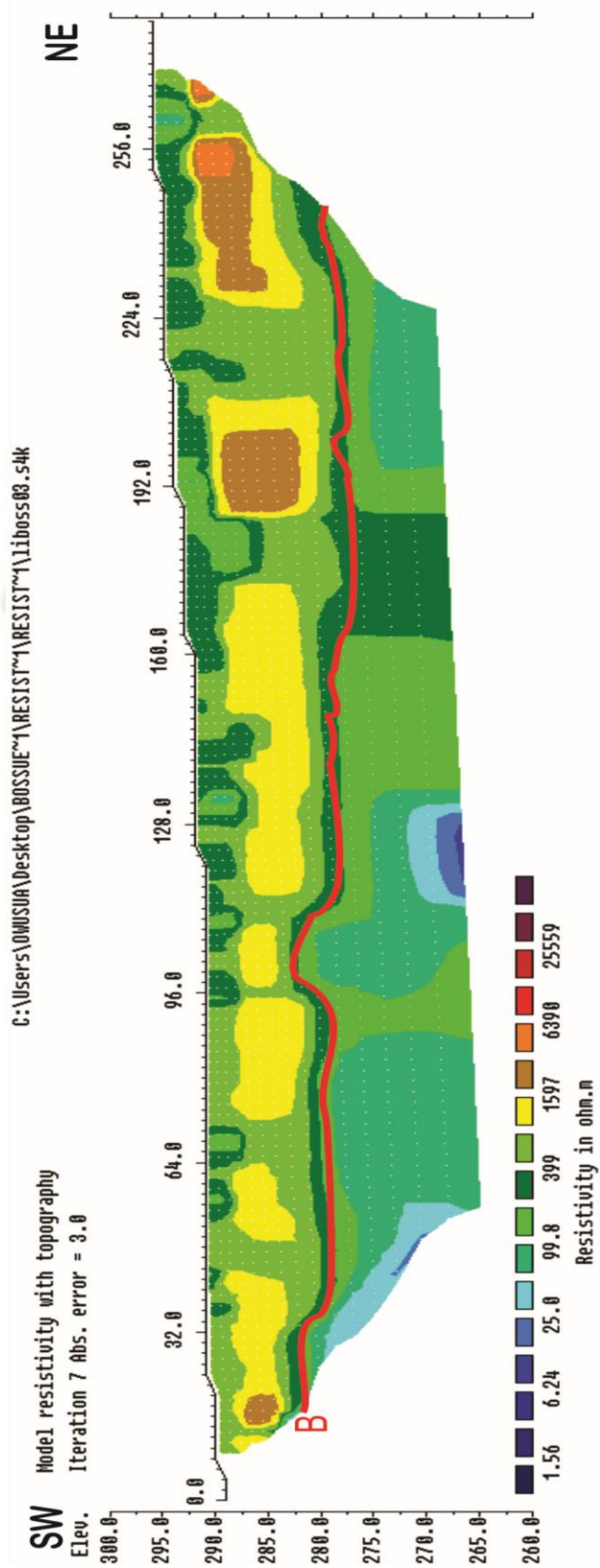
The third layer starts from about 12 m with high resistivity values ranging between 400 and 25000 Ωm indicating the presence of a bedrock which is mainly composed of claystone. At depths greater than or equal to 12 m, resistivity distribution is highly changing laterally; it thus reveals that the basement rock is fractured and shattered. Fractured bedrock zones are imaged below the following distances: 160 to 200 m, 280 to 380 m and 530 to 560 m of the profile. These findings have good correlations with Boamah and Koeberl (2003) results from drill cores (BH1 and BH3). Moreover, the resistivities of northern Bosumtwi suevites are matching with Ries crater suevites in Germany (Ernstson, 1974). The resistivity survey was further carried out along the Nyameani-Boamadumase road from South-West to North-East (Figure 5.3). From the Bosumtwi geological map, this place is free from suevites; it was therefore chosen for cross checking with other profiles which have been carried out in the suevite deposits. The survey was conducted along the road covering a distance of 280 m and crossing a bridge at 50 m.

Model section of profile 3 indicates two layers within the subsurface separated by a boundary B; a little highly resistive near surface followed by a less resistive layer. The thickness of the high resistivity layer is 12 m and the resistivity is greater than 300 Ωm . It is interpreted as dry metasediments comprising phyllite, metagreywackes, shales and schist. The less resistive layer, whose resistivity is less or equal to 300 Ωm could be composed of soils with high moisture content. Since resistivity model results do not show any less resistive zone near the surface, it reveals that this location does not host suevites. Therefore the resistivity results agree with the geological findings.



Dresistivity model section of profile

Figure



3.

Figure D resistivity model section of profile

The direction of geological features in the study area of this project is not known. Hence, other profiles (4, 5 and 6) were surveyed in a direction perpendicular to the base line. Profile 4 has a length of 160 m and was surveyed heading south (figure 5.4). Profiles 4 and 1 crossed each other at 16 and 22 m respectively.

The model section of profile 4 indicates an image of nearly uniform resistivity ($\leq 300 \Omega\text{m}$) distribution within the subsurface. The model section does not show any subsurface strata; which means that, this profile is likely to be in the same direction as subsurface layers. Subsurface along this profile probably has a high moisture content.

In addition to base line, profile 5 was also measured moving Southward. Profiles 5 and 2 crossed each other at 20 and 108 m respectively. Resistivity distribution in the subsurface of profile 5 shows that it is formed by two layers (Figure 5.5). The top layer is more resistive than the underlying layer probably due to the presence of unconsolidated soil in the upper layer which is dry whereas the second layer has a high moisture content. Around 4 m deep, near the beginning and the end of profile 5, and at the depth of 20 m between 44 and 54 m of the profile there are regions of low resistivity ($2 - 25 \Omega\text{m}$). These zones could be suevite deposits. If this low resistivity area at the base is a suevite deposit, then it will be the deepest suevite deposit found in the Bosumtwi crater area.

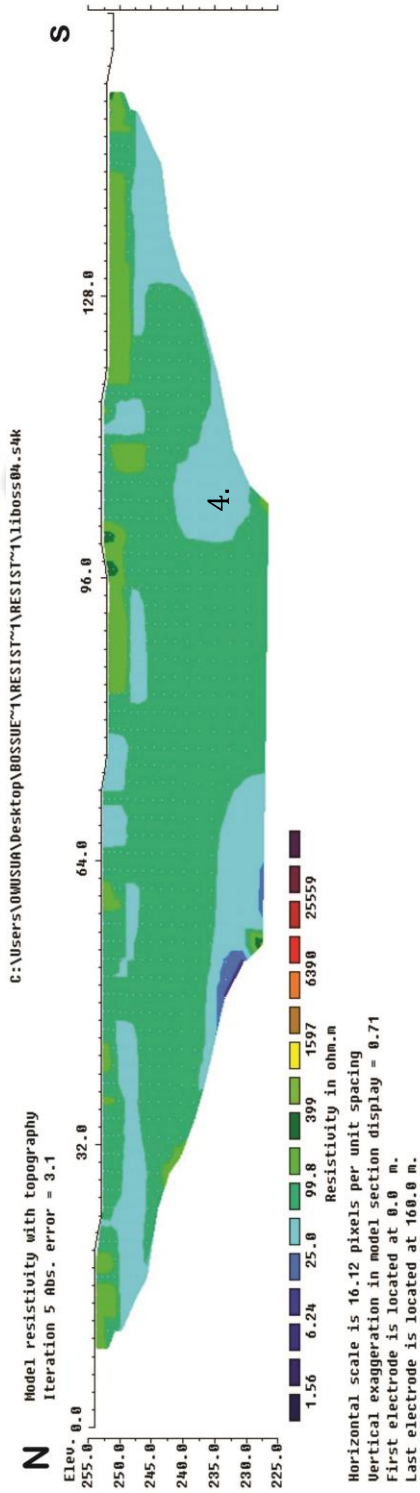


Figure 4. Resistivity model section profile

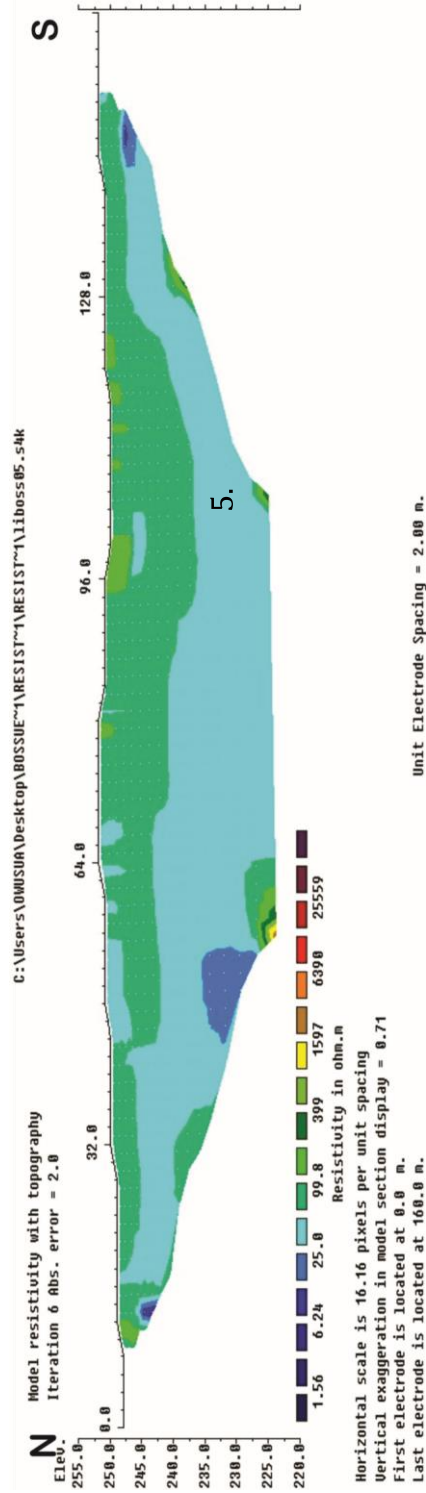
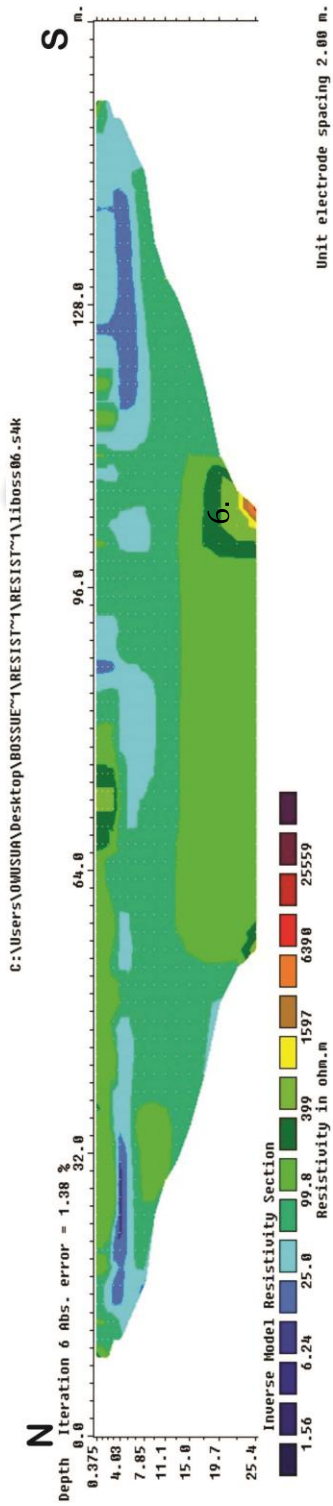


Figure 5. Resistivity model section profile

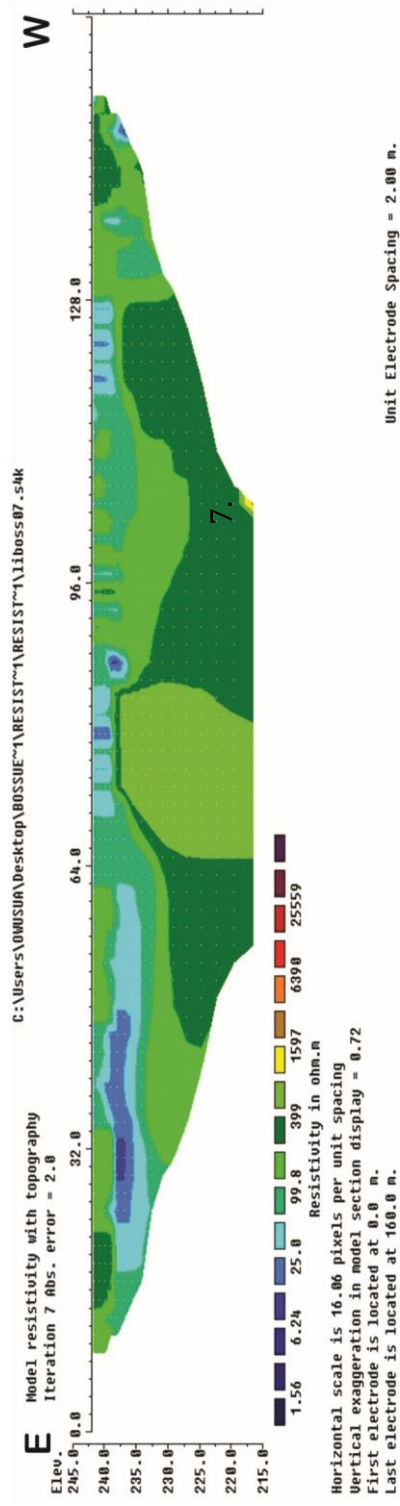
Resistivity model section of profile 6 is also 160 m in length and indicates three layers (Figure 5.6). The first layer is slightly resistive due to dry unconsolidated soil. It is then followed by less resistive second layer which is likely dominated by clay and moisture towards the end, and unevenly intrudes the first layer. The third layer is also resistive slightly high resistivity region and could possibly be the claystone bedrock. At the beginning and the end of the profile around 8 m depth there are low resistivity zones (6 – 25 Ωm). These low resistivity zones are likely to be suevite deposits.

Profile 7, which is the last profile in this project covers 160 m, and was surveyed Westward (Figure 5.7). Profiles 6 and 7 crossed each other at 100 and 20 m respectively. The model section shows that the subsurface is formed by two layers. The first layer is less resistive, with a resistivity value less than 300 Ωm . It is a result of unconsolidated soil with some amount of moisture. The second layer with slightly high resistivity (300 – 1000 Ωm) starts from about 15 m deep. This layer could represent claystone containing some moisture. At the crossing point of profiles 6 and 7 (around 32 m along profile 7) there was a low (6 – 25 Ωm) resistivity which could be suevite deposits.



Dresistivitymodelsectionofprofile

Figure



Dresistivitymodelsectionofprofile

Figure

5.3 Seismic refraction models

Similar to resistivity interpretation, the base survey line was divided into two profiles of 538 m. Figure 5.8 represents the layer model section of profile 1. Profile 1 was surveyed from North-East toward South-West. Probing up to 26 m deep, the layer model reveals that the subsurface is made up of three layers.

The subsurface strata of figure 5.8, reveals that the first layer with thickness less or equal to 4 m, is characterized by relatively low velocities (500 – 800 m/s); it is therefore referred to as unconsolidated and unevenly distributed loose soils containing some moisture. The second layer with a velocity of about 1200 m/s has thickness varying between 2 and 6 m and is interpreted as clayey soil with little high moisture content . The third layer was also delineated with a high velocity of about 2300 m/s. The lithology of this layer is dominated by consolidated country rocks of claystone.

Profile 2 was surveyed from South-West to North-East. The layer models have revealed three layers too. The layer model of figure 5.9 shows that the first layer has a thickness less or equal to 4 m and 400 to 600 m/s velocity. It is then followed by a second layer of thickness varying between 2 and 8 m with an average velocity of 1000 m/s. The second layer therefore overlay a third layer of 1300 m/s velocity. Thus, the varying low velocity of the first layer of profile 2 represents the presence of unconsolidated and uneven distribution of loose soil near the surface. The lithology of the second layer could be formed by clayey soil with little moisture content, while the third layer might be a fractured and shattered country rock of claystone.

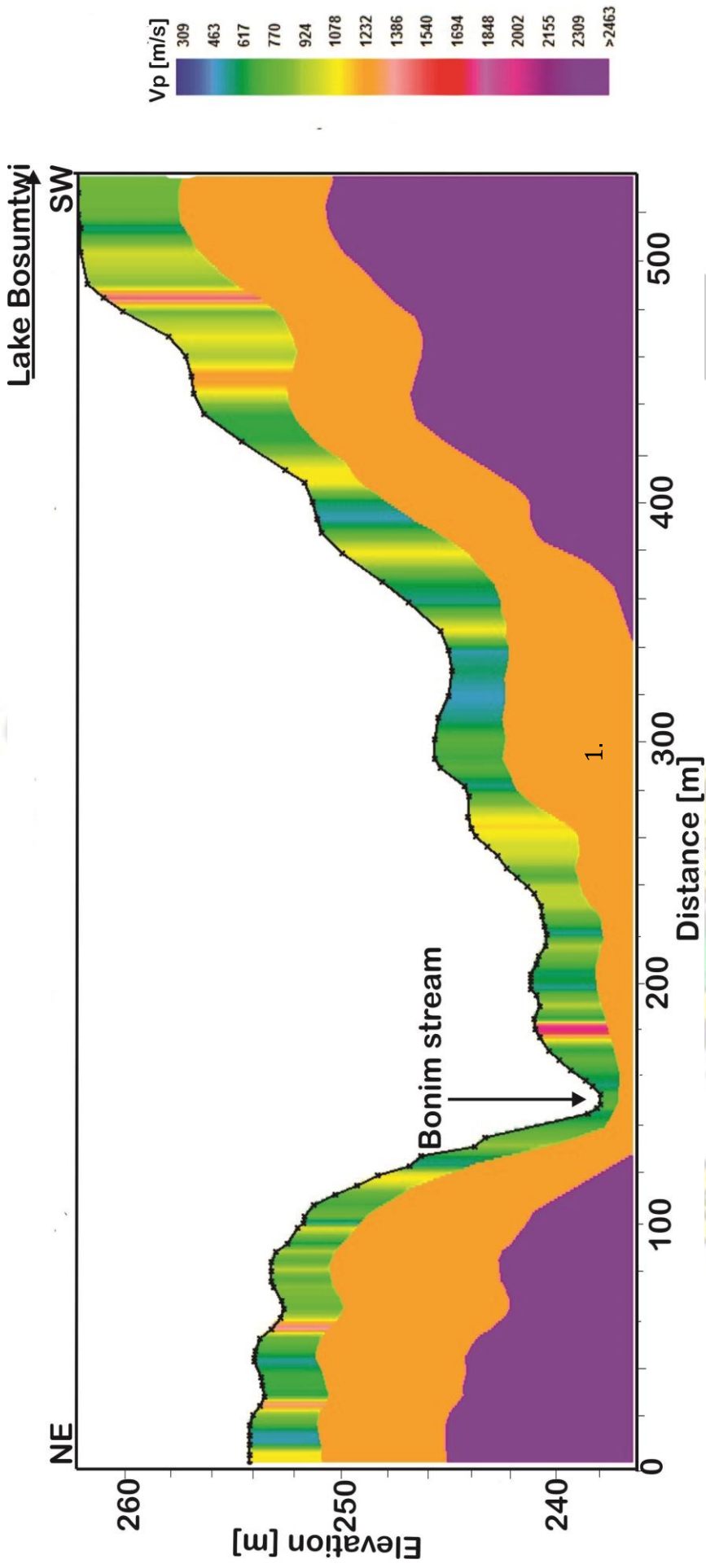


Figure Layer model of profile

5.8:

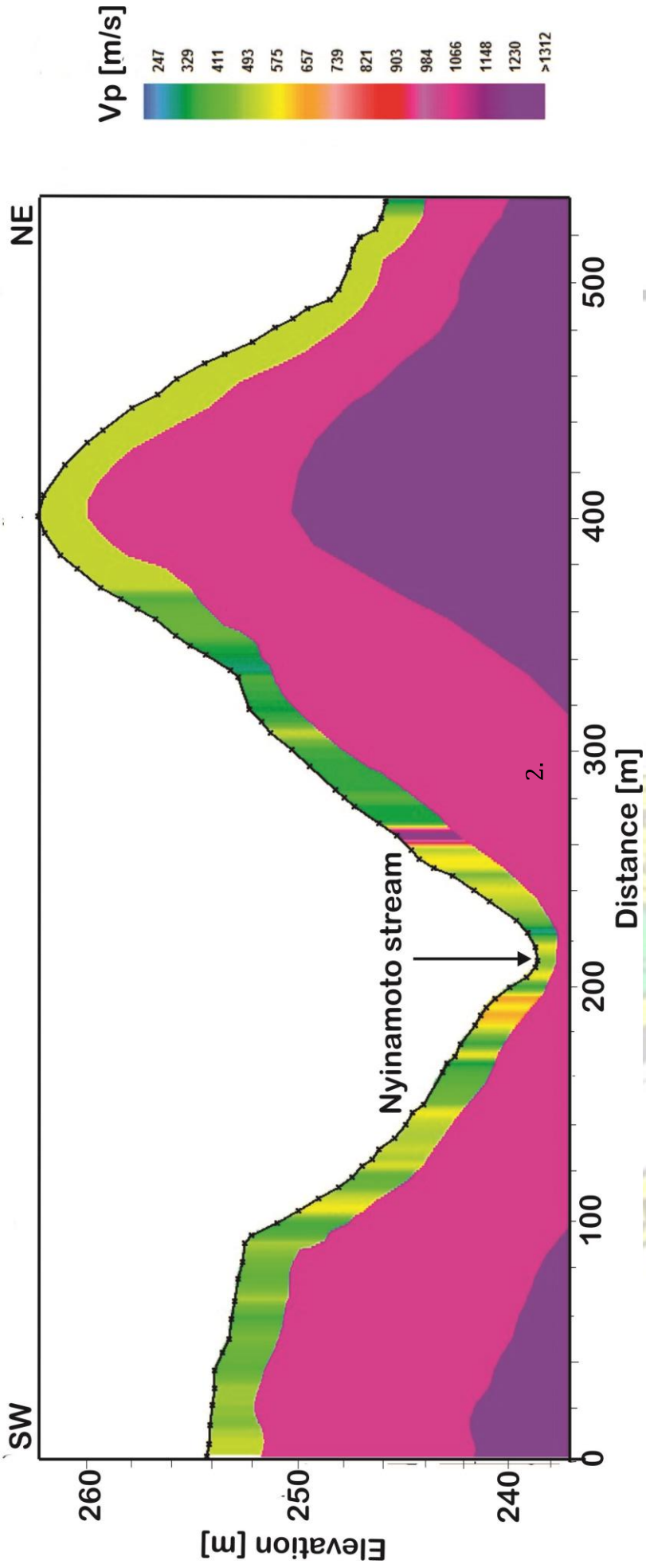
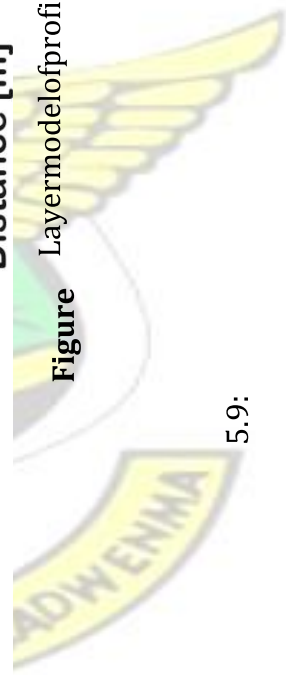


Figure Layer model of profile

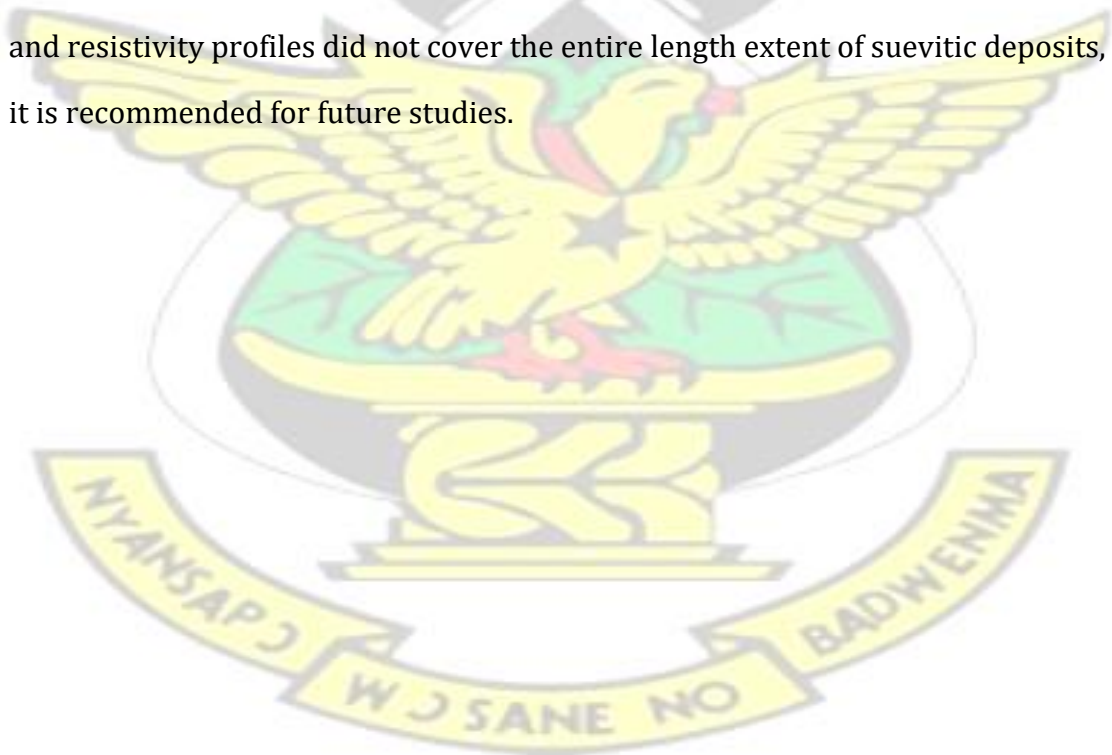


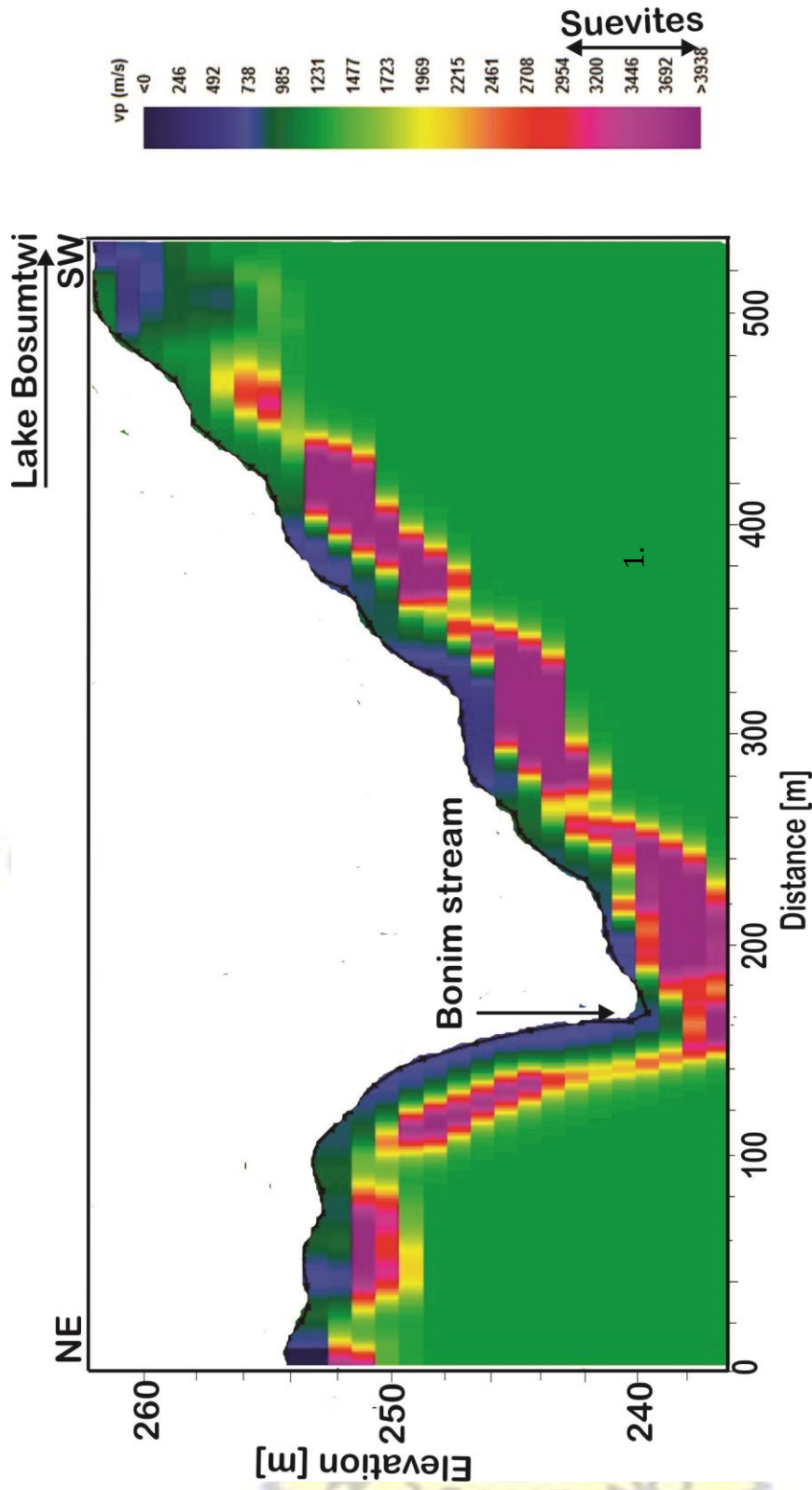
5.9:

Seismic refraction data was further interpreted in terms of tomography in order to know how the lithology of subsurface is controlling the velocity gradient laterally and vertically. Figure 5.10 represents the tomography model section of profile 1.

The tomography model of profile 1 (figure 5.10), revealed high velocity contrast (3000 – 3900 m/s) within the second layer. It was interpreted as suevite deposits which were found within about 8 m depth.

The tomography which complements the layer models of profile 2 (figure 5.11) reveals detailed subsurface formation. There is also a high velocity contrast within the second layer: 3000 to 3900 m/s. This high contrast occurs from the beginning of the profile up to about 380 m and from 480 m until the end of profile. It could be explained as an extent of the suevite deposits that possibly exceed the length of the profile. They were therefore found within 10 m depth. The seismic and resistivity profiles did not cover the entire length extent of suevitic deposits, it is recommended for future studies.





Tomography model profile
Figure

5.10:

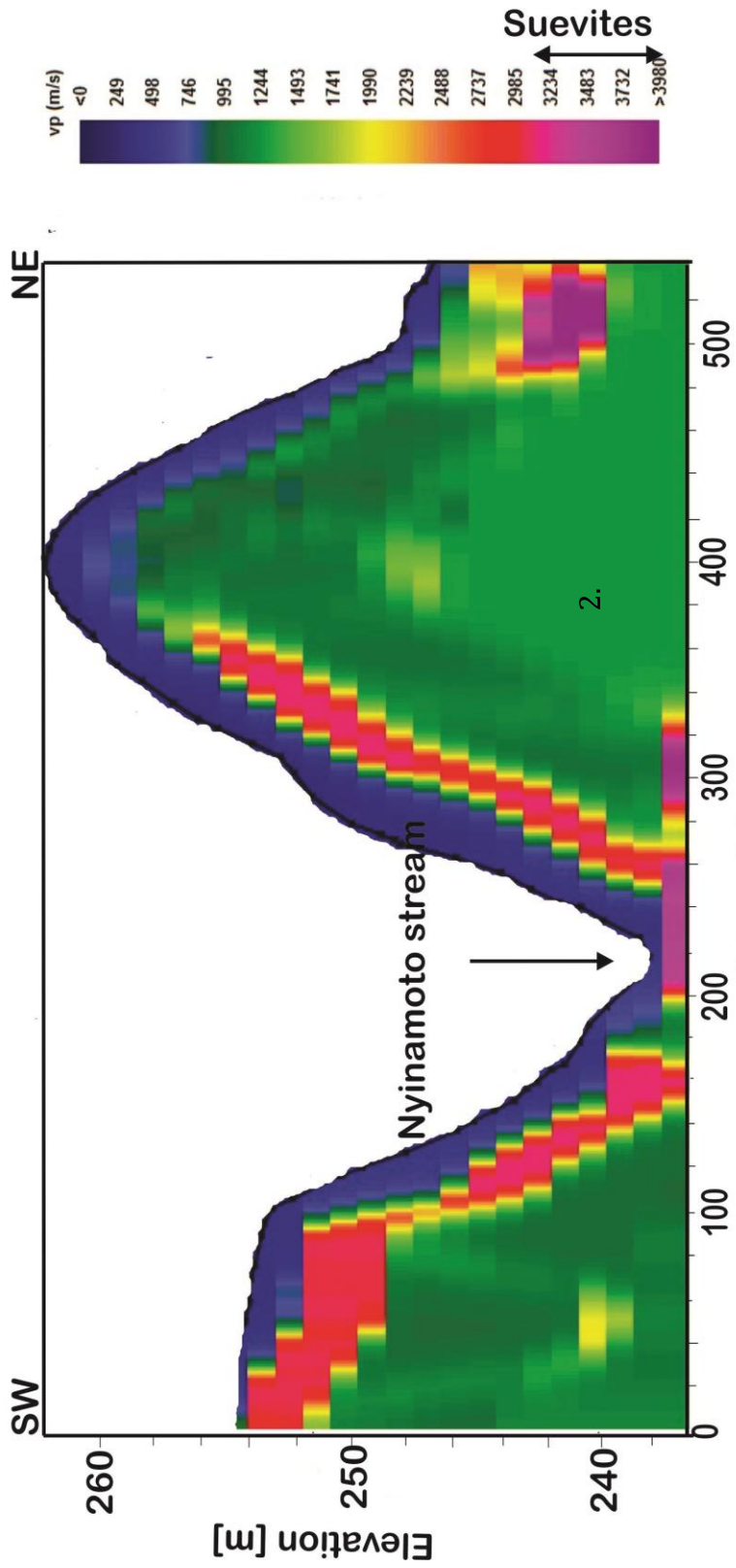


Figure Tomography model profile

5.11:

Chapter 6

CONCLUSION AND RECOMMENDATIONS

6.1 Conclusion

The processed and interpreted seismic refraction and electrical resistivity data, showed suevite deposits and mapped out subsurface strata as well as fractured zones. Suevite deposits were found at depths less or equal to 12 m for all profiles with a low resistivity range of 1.56 to 25 Ωm . Comparatively, the resistivity properties of Northern Bosumtwi suevites are the same as the Ries suevites in Germany (Ernstson, 1974).

Generally, three layers were identified on base line. The top layer with slightly high resistivity (60 – 400 Ωm) has a thickness less or equal to 4 m. It was found that this resistivity is controlled by unconsolidated soil and moist clay. The low resistivity regions, less or equal to 60 Ωm which are mostly dominated by suevite deposits embedded in soils with some amount of moisture was observed in the second layer of profiles 1 and 2. Thickness of these regions are less or equal to 12 m. Beyond 12 m depth, the very high varying resistivity (6000 – 25000 Ωm) was found in the third layer. The high resistivity is the result of a bedrock of claystone, while lateral variation is controlled by fractured zones.

In general case, after changing direction of survey (profiles 4, 5, 6 and 7) the subsurface was imaged to have a low resistivity. This effect could be due to anisotropic behaviour within the subsurface. For profiles 5, 6 and 7, the two layers were mapped out. The top layer for these profiles was less resistive and accounted for by unconsolidated soil with uneven moist clay distribution; while the second layer was generally dominated by claystone and clayey soils.

Profile 3 particularly, has no suevite deposits. Two layers of subsurface were observed; the high resistivity in the near surface is possibly due to the dry metasediments comprising of phyllites and greywackes.

Besides the resistivity findings, the seismic refraction that has been carried out solely on base line was also able to delineate 3 layers of the subsurface and mapped out the suevite deposits. The near surface layer with thickness less or equal to 4 m has P wave velocities ranging between 400 and 800 m/s. Thickness of the second layer however, varies from 4 to 8 m; while P wave velocity varies between 1000 and 1200 m/s. This second layer is dominated by clayey soils. The third layer can be found beneath 12 m depth. Its P-wave velocity varies from 1300 to 2000 m/s. It therefore represents a fractured and shattered basement of claystone.

High velocity contrast (3000 – 3900 m/s) that was observed in the tomography model could be as a result of suevite deposits. This high velocity contrast was found at depths less or equal to 10 m. The P-wave velocity range of northern Bosumtwi suevites is in good correlation with ultrasonic P-wave velocity of suevites in Chicxulub impact structure (Mexico) and Chesapeake Bay impact structure (USA) (Popov et al., 2014).

Therefore, the electrical resistivity tomography and seismic refraction methods have successfully mapped the suevite deposits with low resistivity values and high velocity contrast respectively. Since the study area of this project was covered by cocoa trees, and the surface was covered by cocoa leaves evaporation of the subsurface water was limited. Therefore, the suevites are likely characterized by saturated pores. Fractured zones however, were identified based on slightly low resistivity subsequently low velocity contrast within the basement regions.

6.2 Recommendations

The following recommendations were drawn:

A combination of seismic refraction and electrical resistivity tomography methods have been used successfully in mapping out suevite deposits in the Bosumtwi impact crater area. It is therefore recommended that future researchers in impact cratering studies can use these methods.

Mapping the entire length extent of the northern suevite deposits,

Delineate the Southwest suevite deposits of Bosumtwi impact crater.

KNUST



Bibliography

- Ackermann, H., Godson, R., and Watkins, J. (1975). A seismic refraction technique used for subsurface investigations at Meteor Crater, Arizona. *Journal of Geophysical Research*, 80(5):765–775.
- Affaton, P., Rahaman, M., Trompette, R., and Sougy, J. (1991). The Dahomeyide Orogen: tectonothermal evolution and relationships with the Volta Basin. In *The West African orogens and circum-Atlantic correlatives*, pages 107–122. Springer.
- Aning, A., Tucholka, P., and Danuor, S. (2013a). 2d electrical resistivity tomography (ert) survey using the multi-electrode gradient array at the bosumtwi impact crater, ghana. *Journal of Environmental and Earth Science*, 3(5):12– 27.
- Aning, A., Tucholka, P., and Danuor, S. (2013b). The Bosumtwi Meteorite Impact Crater, Ghana: New results on the impact direction of the meteorite from 2D Electrical Resistivity Tomography (ERT) survey. *International Research Journal of Geology and Mining*, 3(4):147–157.
- Archie, G. E. et al. (1942). The electrical resistivity log as an aid in determining some reservoir characteristics. *Transactions of the AIME*, 146(01):54–62.
- Asihene, K. and Barning, K. (1975). *A contribution to the stratigraphy of the Birimian System of Ghana, West Africa*. Ghana Geological Survey.
- Auken, E. and Christiansen, A. V. (2004). Layered and laterally constrained 2D inversion of resistivity data. *Geophysics*, 69(3):752–761.
- Barton, N. (2007). Rock quality, seismic velocity, attenuation and anisotropy.
- Befus, K. (2010). *Applied geophysical characterization of the shallow subsurface: Towards quantifying recent landscape evolution and current processes in the Boulder Creek watershed, CO*. PhD thesis, University of Colorado at Boulder.

- Bernard, J. (2003). Short note on the depth of investigation of electrical methods. *Source: Google search*, 3(4):5.
- Bertrand-Sarfati, J., Moussine-Pouchkine, A., Affaton, P., Trompette, R., and Bellion, Y. (1991). Cover sequences of the West African Craton. In *The West African orogens and circum-atlantic correlatives*, pages 65–82. Springer.
- Boamah, D. and Koeberl, C. (2003). Geology and geochemistry of shallow drill cores from the Bosumtwi impact structure, Ghana. *Meteoritics & Planetary Science*, 38(8):1137–1159.
- Chao, E. (1968). Pressure and temperature histories of impact metamorphosed rocks—based on petrographic observations. *Shock metamorphism of natural materials*, pages 135–158.
- Dahlin, T. and Zhou, B. (2006). Multiple-gradient array measurements for multichannel 2D resistivity imaging. *Near Surface Geophysics*, 4(2):113–123.
- Danuor, S., Aning, A., Pohl, J., Karp, T., and Berckhemer, H. (2013). Geophysical characteristics of the bosumtwi impact crater from seismic, gravity and magnetic measurements. *European Scientific Journal*, 9(15).
- Davis, D., Hirdes, W., Schaltegger, U., and Nunoo, E. (1994). U pb age constraints on deposition and provenance of Birimian and gold-bearing Tarkwaian sediments in Ghana, West Africa. *Precambrian Research*, 67(1):89–107.
- Duodu, J. A. (2009). *Geological Map of Ghana 1: 1 000 000*. Geological Survey Department.
- Eisenlohr, B. and Hirdes, W. (1992). The structural development of the early Proterozoic Birimian and Tarkwaian rocks of southwest Ghana, West Africa. *Journal of African Earth Sciences (and the Middle East)*, 14(3):313–325.
- Ellis, R. and Oldenburg, D. (1994). Applied geophysical inversion. *Geophysical Journal International*, 116(1):5–11.

- Ernstson, K. (1974). Structure of Ries crater from geoelectric depth soundings. *Journal of Geophysics-Zeitschrift Fur Geophysik*, 40(5):639–659.
- Everett, M. E. (2013). *Near-surface applied geophysics*. Cambridge University Press.
- Ferriere, L., Koeberl, C., and Reimold, W. U. (2007). Drill core LB-08A, Bosumtwi impact structure, Ghana: Petrographic and shock metamorphic studies of material from the central uplift. *Meteoritics & Planetary Science*, 42(45):611–633.
- French, B., Koeberl, C., Gilmour, I., Shirley, S., Dons, J., and Naterstad, J. (1997). The gardnos impact structure, norway: Petrology and geochemistry of target rocks and impactites. *Geochimica et Cosmochimica Acta*, 61(4):873–904.
- Garvin, J. B., Schnetzler, C. C., and Grieve, R. A. (1992). Characteristics of large terrestrial impact structures as revealed by remote sensing studies. *Tectonophysics*, 216(1):45–62.
- Gentner, W., Storzer, D., and Wagner, G. (1969). New fission track ages of tektites and related glasses. *Geochimica et Cosmochimica Acta*, 33(9):1075– 1081.
- Glass, B. P. (1969). Chemical composition of Ivory Coast microtektites. *Geochimica et Cosmochimica Acta*, 33(9):1135–1147.
- Green, R. and Chetty, P. (1990). Seismic refraction studies in the basement of the Vredefort structure. *Tectonophysics*, 171(1):105–113.
- Griffiths, D. and Barker, R. (1993). Two-dimensional resistivity imaging and modelling in areas of complex geology. *Journal of Applied Geophysics*, 29(3):211–226.
- Haeni, F. (1986). Application of seismic refraction methods in groundwater modeling studies in New England. *Geophysics*, 51(2):236–249.

- Hastings, D. A. (1982). On the tectonics and metallogensis of West Africa: a model incorporating new geophysical data. *Geoexploration*, 20(3):295–327.
- Hunze, S. and Wonik, T. (2007). Lithological and structural characteristics of the Lake Bosumtwi Impact Crater, Ghana: Interpretation of acoustic televiwer images. *Meteoritics & Planetary Science*, 42(4-5):779–792.
- Jones, W. (1985). Chemical analyses of Bosumtwi Rater target rocks compared with the Ivory Coast tektites. *Geochimica et Cosmochimica Acta*, 49(12):2569–2576.
- Jones, W. B., Bacon, M., and Hastings, D. A. (1981). The Lake Bosumtwi Impact Crater, Ghana. *Geological Society of America Bulletin*, 92(6):342–349.
- Jongmans, D. and Garambois, S. (2007). Geophysical investigation of landslides: a review. *Bulletin de la Soci'et'e g'eologique de France*, 178(2):101–112.
- Junner, N. (1940). *Geology of the Gold Coast and Western Togoland with revised geological map*. Published under the authority of His Excellency Sir Arnold Hodson, Governor of the Gold Coast.
- Karp, T., Milkereit, B., Janle, P., Danuor, S. K., Pohl, J., Berckhemer, H., and Scholz, C. A. (2002). Seismic investigation of the Lake Bosumtwi Impact Crater: Preliminary results. *Planetary and Space Science*, 50(7):735–743.
- Kearey, P., Brooks, M., and Hill, I. (2009). An introduction to geophysical exploration.
- Kesse, G. O. (1985). The mineral and rock resources of Ghana.
- Kno"del, K., Lange, G., and Voigt, H.-J. (2007). *Environmental geology: handbook of field methods and case studies*. Springer Science & Business Media.
- Koeberl, C. (1986). Geochemistry of tektites and impact glasses. *Annual Review of Earth and Planetary Sciences*, 14:323–350.

- Koeberl, C. (1994). Tektite origin by hypervelocity asteroidal or cometary impact. *Large Meteorite Impacts and Planetary Evolution*, 293:133.
- Koeberl, C., Bottomley, R., Glass, B. P., and Storzer, D. (1997). Geochemistry and age of Ivory Coast tektites and microtektites. *Geochimica et Cosmochimica Acta*, 61(8):1745–1772.
- Koeberl, C., Milkereit, B., Overpeck, J. T., Scholz, C. A., Amoako, P. Y., Boamah, D., Danuor, S., Karp, T., Kueck, J., Hecky, R. E., et al. (2007). An international and multidisciplinary drilling project into a young complex impact structure: The 2004 ICDP Bosumtwi Crater Drilling Project—an overview. *Meteoritics and Planetary Science*, 42:483–511.
- Koeberl, C., Reimold, W., Blum, J., and Chamberlain, C. P. (1998). Petrology and geochemistry of target rocks from the Bosumtwi impact structure, Ghana, and comparison with Ivory Coast tektites. *Geochimica et Cosmochimica Acta*, 62(12):2179–2196.
- Lacroix, A. (1934). Sur la découverte de tectites à la Côte d'Ivoire. *Comptes Rendus Academie des Sciences, Paris*, 199:1539–1542.
- Leube, A., Hirdes, W., Mauer, R., and Kesse, G. O. (1990). The early Proterozoic Birimian Supergroup of Ghana and some aspects of its associated gold mineralization. *Precambrian Research*, 46(1):139–165.
- Littler, J., Fahey, J., Dietz, R. S., and Chao, E. (1961). Coesite from the Lake Bosumtwi Crater, Ashanti, Ghana. *GSA Special Paper*, 68:218.
- Loke, M. (1999). Electrical imaging surveys for environmental and engineering studies. *A practical guide to*, 2.
- Loke, M. and Dahlin, T. (2002). A comparison of the Gauss–Newton and quasiNewton methods in resistivity imaging inversion. *Journal of Applied Geophysics*, 49(3):149–162.

- Loke, M. and Lane Jr, J. W. (2004). Inversion of data from electrical resistivity imaging surveys in water-covered areas. *Exploration Geophysics*, 35(4):266–271.
- Maclaren, M. (1931). Lake Bosumtwi, Ashanti. *Geographical Journal*, pages 270–276.
- Melosh, H. J. (1989). Impact cratering: A geologic process. *Research supported by NASA. New York, Oxford University Press (Oxford Monographs on Geology and Geophysics, No. 11), 1989, 253 p., 1.*
- Milsom, J. (2003). *Field Geophysics*, volume 25. John Wiley and Sons.
- Moon, P. and Mason, D. (1967). The geology of 1/4 field sheets 129 and 131. *Bompata SW and NW Ghana Geological Survey Bulletin*, 31:1–51.
- Olayinka, A. and Yaramanci, U. (2000). Use of block inversion in the 2D interpretation of apparent resistivity data and its comparison with smooth inversion. *Journal of Applied Geophysics*, 45(2):63–81.
- Oldenburg, D. W. and Li, Y. (1999). Estimating depth of investigation in DC resistivity and IP surveys. *Geophysics*, 64(2):403–416.
- Pilkington, M. and Grieve, R. (1992). The geophysical signature of terrestrial Impact Craters. *Reviews of Geophysics*, 30(2):161–181.
- Plado, J., Pesonen, L., Koeberl, C., and Elo, S. (2000). The Bosumtwi meteorite impact structure, Ghana: A magnetic model. *Meteoritics and Planetary Science*, 35:723–732.
- Plado, J., Pesonen, L. J., Elo, S., Puura, V., and Suuroja, K. (1996). Geophysical research on the kaärdla impact structure, Hiiumaa Island, Estonia. *Meteoritics & Planetary Science*, 31(2):289–298.
- Popov, Y., Mayr, S., Romushkevich, R., Burkhardt, H., and Wilhelm, H. (2014). Comparison of petrophysical properties of impactites for four meteoritic impact structures. *Meteoritics & Planetary Science*, 49(5):896–920.

- Rae, J. (2009). Technical Report on the Kwabeng Gold Project.
- Reimold, W. U., Brandt, D., and Koeberl, C. (1998). Detailed structural analysis of the rim of a large, complex impact crater: Bosumtwi Crater, Ghana. *Geology*, 26(6):543–546.
- Reynolds, J. M. (2011). *An introduction to applied and environmental geophysics*. John Wiley & Sons.
- Scholz, C. A., Karp, T., Brooks, K. M., Milkereit, B., Amoako, P. Y., and Arko, J. A. (2002). Pronounced central uplift identified in the Bosumtwi impact structure, Ghana, using multichannel seismic reflection data. *Geology*, 30(10):939– 942.
- Smith, T., Hoversten, M., Gasperikova, E., and Morrison, F. (1999). Sharp boundary inversion of 2D magnetotelluric data. *Geophysical Prospecting*, 47(4):469–486.
- Spray, J. and Hines, J. (2009). Earth impact database. *Planetary and Space Science Centre, University of New Brunswick, Canada*. <http://www.unb.ca/passc/ImpactDatabase/index.html> (March 2010).
- Stoßler, D. and Grieve, R. (1994). Classification and nomenclature of impact metamorphic rocks: A proposal to the IUGS subcommission on the systematics of metamorphic rocks. In *Lunar and Planetary Science Conference*, volume 25, page 1347.
- Stummer, P., Maurer, H., and Green, A. G. (2004). Experimental design: Electrical resistivity data sets that provide optimum subsurface information. *Geophysics*, 69(1):120–139.
- Telford, W. M., Geldart, L. P., and Sheriff, R. E. (1990). *Applied geophysics*, volume 1. Cambridge University Press.
- Wagner, R., Reimold, W. U., and Brandt, D. (2002). Bosumtwi Impact Crater, Ghana: A remote sensing investigation. In *Impacts in Precambrian shields*, pages 189–210. Springer.

Wenner, F. (1912). A method of measuring earth resistivity. US Bureau of Standards Bulletin, 12: 469-478. Zohdy, AAR, 1974, electrical methods. *Applications of Surface Geophysics to Groundwater Investigations, Book, 2.*

Woodfield, P. (1966). The geology of the 1/4 field sheet 91. *Fumso NW Ghana Geological Survey Bulletin*, 30:1–66.

Wright, J. B. (1986). *Geology and mineral resources of West Africa*. Springer Science & Business Media.

Yao, Y., Murphy, P., and Robb, L. (2001). Fluid characteristics of Granitoidhosted Gold Deposits in the Birimian Terrane of Ghana: A fluid inclusion microthermometric and raman spectroscopic study. *Economic Geology*, 96(7):1611–1643.

Appendix

Used softwares

RES2DINV: Resistivity data processing

ReflexW: Seismic data processing

Coral Draw X5: Graphics

MapInfo10.5.Discover 11.1: Location of study area,

Linux: Writing research project.